EFFECT OF SURFACE ENVIRONMENT ON ENERGY RELAXATION DYNAMICS IN PHOTO-EXCITED NANOCRYSTALS

A Dissertation

by

SOURAV MAITI

Submitted to the Office of Graduate and Professional Studies of
Texas A&M University
in partial fulfillment of the requirements for the degree of

MASTER OF SCIENCE

Chair of Committee,	Dong Hee Son
Committee Members,	Christian Hilty
	Igor Roshchin
Head of Department,	David H. Russell

December 2013

Major Subject: Chemistry

ABSTRACT

The optical properties of semiconducting nanocrystals have considerable application in various fields such as biological imaging, light emitting devices and solar cells. Due to high surface to volume ratio surface structure has a profound effect on the exciton quantum yield and charge carrier dynamics of these nanocrystals. Surface imperfections or surface defects often decrease the exciton quantum yield by trapping the charge carriers and thus affect relaxation dynamics. Surface binding surfactants play an important role in determining optical properties and exciton dynamics as they can remove surface defects through passivation and they can also introduce new trap sites.

Transition metal doped semiconducting nanocrystals especially Mn-doped in II-VI semiconducting host show stoke shifted Mn-emission with high Mn-emission quantum yield applicable in light emitting devices, biological imaging and sensors. Although Mn-emission was found to depend on surface effects, the underlying mechanism and dynamics was not explored in great detail. Thiols are important class of surfactants used to passivate nanocrystals especially to make water soluble nanocrystals. Thiols are hole trapping surfactants and known to quench the emission in CdSe or CdS nanocrytals. In our study, we examined the effect of hole trapping ligand octanethiol on the Mn-luminescence quantum yield and exciton dynamics in Mn-doped CdS/ZnS nanocrystals. Surprisingly Mn-luminescence quantum yield was found to increase in presence of octanethiol in contrary to undoped nanocrystals where octanethiol almost quenched the exciton emission. Combining transient absorption measurements with

steady state Mn-photoluminescence and Mn-lifetime measurements, we confirmed the existence of an energy transfer process from octanethiol created hole traps to Mn that enhances the Mn-photoluminescence.

Apart from studying the effect of surface environment in exciton relaxation dynamics in Mn-doped nanocrystals, we have studied the effect of surfactant and solvent on the spin relaxation dynamics in magnetic nanocrystals through transient Faraday rotation measurements. The spin-lattice relaxation rate in spherical Fe_3O_4 nanocrystals depends on the functional group and binding nature of the surfactant. Also, the solvent affects the spin-lattice relaxation rate only when they can access the surface of the nanocrystals. Therefore, thick surfactant passivation prevents the approach of the solvent molecules resulting spin-lattice relaxation rate independent of solvent environment.

To my family and friends

ACKNOWLEDGEMENTS

I would like to thank my advisor Dr. Dong Hee Son for his constant help and support. I would also like to thank my committee members Dr. Hilty and Dr. Roshchin for providing their valuable time for my dissertation. I also thank my old committee member Dr. Batteas for his advice and time. I take this opportunity to thank Department of Chemistry, Texas A&M University for giving me the chance to study here. I thank all the departmental staff especially Sandy Manning for the help and prompt response and university writing center for their help to complete my thesis. I thank Dr. Lisa Pérez, Laboratory of Molecular Simulations, for some helpful sessions to understand some of the theoretical aspects of my research. I also want to thank my all my lab members for their help and suggestions during my research especially Hsiang-Yun Chen for being an outstanding senior student. She helped me in each and every aspect of my daily research life. I also thank my friends and family for their understanding and support. Finally, I want to thank my fiancé Shaoni Nandi for her mental support that strengthens me in my difficult times.

TABLE OF CONTENTS

LIST OF FIGURES

LIST OF TABLES

CHAPTER I

INTRODUCTION

Semiconductor nanocrystals have interesting opto-electronic properties quite different from the bulk counterpart.[1-4] For instance, due to confinement of the charge carriers semiconductor nanocrystals possess quantized energy levels in contrary to the bulk. Excitation within the nanocrystals creates electron-hole pair or exciton. Confinement of charge carriers (excitons) leads to quantization of energy levels that gives rise to size dependent optical spectra and adds new mechanisms to charge carrier (electron or hole) relaxations.[5-8] These new opto-electronic properties have found application in solar cells, opto-electronic devices and bio-imaging.[9-14] Not only the size, the shape and the composition of the nanocrystals can also modify the opto-electonic properties.[15] Extensive research is going on to control size, shape and composition of nanocrystals for harvesting these properties and also to find out the underlying mechanisms of charge carrier dynamics form spectroscopic point of view. [4,16-19]

Transition metal doped semiconducting nanocrystals are new type of materials where transition metal ion (Mn, Cu etc.) is doped in the nanocrystal lattice as an impurity.[20-24] Doping modifies charge carrier dynamics due to exciton-dopant coupling and introduces new opto-electronic properties that have potential applications in light emitting devices, biological imaging and spintronics.[20,23,25-31] As an example, in Mn-doped nanocrystals the exciton emission is quenched by fast energy transfer to Mn which leads to red shifted emission resulting from spin-forbidden d-d transition in

Mn.[23,27,32] Due to fast exciton to Mn energy transfer and slow relaxation of Mn, in Mn-doped nanocrystals Mn has been used as an energy reservoir.[33]

As stated earlier, the size, shape and composition are some of the important parameters that govern nanocrystal properties.[15] Also, for nanocrystals due to high surface to volume ratio the surface atoms play an important role in determining exciton relaxation dynamics.[34-36] Defect states arising due to unbalanced valence of the surface atoms lead to trapping of the charge carriers and add new pathways for exciton relaxation. The surface bound surfactants which are necessary to passivate nanocrystals to make them stable in solution preventing aggregation play an important role by removing the surface defects (or traps) through co-ordinating with the surface atoms. Also, the surfactants can introduce new surface traps depending on the nature of the surfactants. For semiconducting nanocrystals trapping of the charge carriers are the major process reducing quantum yield. There are both electron trapping and hole trapping surfactants which modifies the exciton dynamics in different ways.[37] Thus surfactants have a great influence on the exciton dynamics and emission properties of semiconducting nanocrystals.

Apart from affecting the exciton dynamics in semiconductor nanocrystals, the magnetic behavior of the magnetic nanocrystals is also greatly influenced by the surface environment especially by the surface binding surfactants.[38-44] Magnetic properties such as coercitivity and static magnetization of nanocrystals are influenced by surfactants.[44] Also, certain surface passivating surfactants are found to improve magnetization on the surface through strong binding with the surface magnetic atoms.[41]

Therefore, surfactants play a vital role in controlling charge carrier dynamics and magnetic properties both in semiconductor nanocrystals and magnetic nanocrystals. However, the role of the surfactants on the exciton dynamics is not well understood in doped semiconductor nanocrystals, although it can be envisaged that surfactants will have an important role controlling the dopant emission and exciton dynamics. Also, in magnetic nanocrystals surfactant dependent spin relaxation is not elucidated in great detail. This thesis focuses on the role of surface environment on energy relaxation dynamics of two different nanocrystals. We have investigated the role of surfactants on exciton dynamics and Mn-luminescence in Mn-doped CdS/ZnS core/shell nanocrystals. On the other hand, we have studied effect of solvent and surfactant on the spin relaxation dynamics of Fe_3O_4 nanocrystals.

Pump-probe transient absorption measurement is used to examine the exciton dynamics in Mn-doped CdS/ZnS nanocrystals. Transient absorption is a well-known technique to resolve charge carrier dynamics occurring in ultrafast time scale in semiconducting nanocrystals.[5,8,35,37,45-51] Recently, we have used this technique to explore exciton to Mn energy transfer dynamics in Mn doped CdS/ZnS nanocrystals.[32,52] Now, we have extended the technique to investigate surfactant dependence of exciton dynamics and Mn-emission in these nanocrystals. On the other hand, pump-probe Faraday rotation technique is used to find out the role of surfactants and solvents on spin-relaxation dynamics in super-paramagnetic iron oxide nanocrystals. Earlier, this technique was used in our group to study size and composition dependent spin-relaxation dynamics in iron oxide and cobalt ferrite nanocrystals which revealed

important of surface atoms on the relaxation dynamics.[53,54] Therefore, it was interesting to show how the surfactant and solvents affect the spin relaxation dynamics.

The dissertation is organized as follows. Chapter II summarizes all the necessary literatures. All the experimental procedures including synthesis, characterization of the nanocrystals, steady state and time resolved measurements are discussed in chapter III. Chapter IV discusses the effect of hole trapping surfactant octanethiol on the exciton dynamics of Mn-doped CdS/ZnS nanocrystals. Chapter V is about the effect of solvent and surfactant on the spin relaxation dynamics of Fe_3O_4 nanocrystals. Finally, chapter VI discusses about future aspects of the current study.

CHAPTER II

BRIEF DISCUSSION ABOUT RELEVANT LITERATURE

2.1 Energy Relaxation Dynamics in Semiconducting Nanocrystals

2.1.1 Electronic Structure of Semiconducting Nanocrystals

Bulk Semiconductors are comprised of valence band and conduction band separated by band-gap energy. The valence band is filled with electrons while the conduction band is empty. The minimum energy required to excite an electron from valence band to conduction band is the band-gap. Excitation of an electron to the conduction band produces an electron-hole pair, known as the exciton. The electron and hole act as the charge carriers in the semiconductors. The separation distance between the electron and the hole is known as the Bohr radius. Table 2.1 lists Bohr radius for some of the well-known nanocrystals which are mostly in the nm length scale.[55]

Semiconductor	Exciton Bohr radius (nm)
CdSe	6
InAs	36
CuCl	0.7

Table 2.1 Exciton Bohr radii of semiconducting nanocrystals.

The valence and conduction band are continuous in the bulk semiconductors. This situation changes dramatically when the size of the semiconductor narrows down to

the Bohr radius. In this nanometer size domain the semiconducting nanocrystals, also known as quantum dots start to show quantum effects. The charge carriers become confined in in all three directions (3D confinement) compared to the bulk, which results in discretizes the valence and conduction bands. The band-gap energy becomes size and shape dependent and below the Bohr radius, the band-gap energy increases than the bulk. Thus the absorption and emission spectra of the semiconducting nanocrystals become size and shape dependent. Figure 1 in reference 48 shows the absorption (black line) and emission spectra (grey line) along with the valence and conduction band energy diagram of spherical CdSe quantum dots. The discrete transitions in the absorption spectra with $1S_{3/2} - 1S_e$ is the band-edge transition.[48] Immediately after excitation (<1ps) the charge carriers relax to the band-edge and recombines to give exciton emission.

2.1.2 Exciton Dynamics in Semiconducting Nanocrystals

In bulk semiconductor, the photo-excited hot electron in the conduction band relaxes to the band-edge by providing the excess energy to lattice phonons. As the conduction band is continuous, the electron does not suffer from any energy mismatch with the phonon. However, in the nanocrystal due to discretization of the conduction band, the electron cannot give away any amount of energy. Also, the energy separation between the conduction band states (~ fraction of eV) is much larger than the typical phonon energy (~0.02eV). Therefore, the electronic relaxation from one level to the other requires ~10 phonons at a time which is an improbable process. This gives rise to "phonon bottleneck" which means the electron relaxation in nanocrystals should be

much slower than the bulk.[15,56] However, experiments have revealed very fast (~ps) energy relaxation of electrons in the nanocrystals, which involves different mechanisms. Hole energy levels in the valence band; on the other hand, has small energy spacing and thus the hole can relax through phonons. The fast intraband relaxation of electrons is proposed through an Auger type mechanism, where the excited electron gives its energy to the hole through electron-hole coupling and the hole then relaxes through phonons. Another important aspect of nanocrystals is the high surface to volume ratio. For small nanocrystals most of the atoms are on the surface and the surface atoms suffer from lack of co-ordination. Surface imperfections or defects lead to new relaxation mechanism for the charge carriers by introducing trapping of the charge carriers.[15,57]

The charge carrier relaxation processes are generally in the ultrafast time scale and pump-probe transient absorption is a widely used technique to elucidate ultrafast relaxation processes. In this method a pump beam is used to create exciton in the nanocrystals and the population of the excitonic state is probed with a probe beam as a function of pump-probe delay time. By recording change in absorption with and without the pump beam with delay time ($\Delta OD\ (t) = OD_{pump\ on} - OD_{pump\ off}$) one monitors the dynamics of the charge carriers probed. In typical pump-probe experiments one either probes at the band-edge, the near-IR and IR regions. Probing at the band-edge provides relaxation dynamics of the electron at the band-edge, which is known as bleach recovery dynamics. [7,36,57-60] When probed at near-IR, mixed dynamics having contributions from both the electron and hole is observed where intraband transition of charge carriers is monitored. Transient absorption measurements have provided valuable information

about charge carrier relaxation. Intraband relaxation of excited electron takes place in sub-ps to ps timescale whereas electron trapping time is about hundreds of ps. For, hole trapping the typical time is about few ps. Transient absorption measurements have also been utilized to find out effect of different surfactants and trapping agents and dopants on the exciton dynamics. For instance, effect of electron and hole trapping ligands on exciton dynamics has been reported by many groups.[37,61] Also, exciton-Mn energy transfer time is precisely determined in Mn-doped CdS/ZnS core/shell nanocrystals using transient absorption measurements.[32] These will be discussed in more details in the subsequent sections.

2.2 Effect of Surfactant on Exciton Dynamics

Surface passivating surfactants are integral part of nanocrystal structure. They provide stability to the nanocrystals by preventing aggregation. During synthesis, surfactants control the nucleation and growth kinetics of the nanocrystals. Also, in the nanocrystals they remove the surface defects by binding with the surface atoms. Importantly, surfactants can also create new trap sites which can add complexity in the exciton dynamics.[34,62] Some of the commonly used surfactants are phosphine oxides (tri-n-octyl phosphine oxide, TOPO), phosphines (Trioctylphosphine, TOP), amines (oleyl amine), carboxylic acids (oleic acid) and thiols (mercapto propionic acid, octanethiol). The effect of surfactants on exciton dynamics is well documented and is discussed in chapter 4.

2.3 Mn-Doped Nanocrystals: Exciton-Mn Energy Transfer Dynamics

As discussed in the introduction, the exciton-Mn energy transfer excites Mn and leads to the spin-forbidden 4T1 $\rightarrow$ 6A1 transition in Mn which leads to Mn-emission. Wavefunction overlap between exciton and Mn determines the energy transfer rate between the exciton and Mn.[20] The stronger the overlap the faster is the relaxation. In undoped nanocrystals the exciton recombines in the order of ns to have exciton photoluminescence (PL). Except for the exciton recombination, many other competing processes like electron or hole trapping are feasible. Incomplete coordination on the surface is the major source of surface defects which leads to trapping. In Mn-doped nanocrystals exciton-Mn energy transfer opens up another channel for exciton relaxation. The energy transfer excites the Mn d-d transition and the Mn relaxes through $^4T_1 \rightarrow {}^6A_1$ spin-forbidden transition. The advantage of Mn-emission compared to exciton emission is that Mn-emission is environment insensitive and less prone to get affected by surface defects.[63]

Whether the mechanism of exciton-Mn energy transfer is Förster or Dexter type is still uncertain. A dipole mediated Förster type mechanism has been proposed by Yang et. al.[64] However, it is based on some assumptions and need more justifications. Irrespective of the exact mechanism, the energy transfer rate depends on the exciton-Mn wavefunction overlap which can be tuned by changing the position of Mn in a core/shell nanocrystal structure.[32,64]

2.4 Photo-induced Demagnetization and Magnetization Recovery in Fe_3O_4 Nanocrystals

Magnetization recovery in photo-excited Fe_3O_4 nanocrystals occurs through flow of energy and momentum from spins to the lattice degrees of freedom. This spin-lattice relaxation was monitored using pump-probe Faraday rotation technique. When plane polarized light passes through a magnetic media, the plane of polarization gets rotated, known as Faraday effect. The degree of rotation is proportional to the magnetization in the sample. Monitoring the change in Faraday rotation angle, change in magnetization can be measured in real time. The Faraday rotation technique along with details of magnetism and magnetization dynamics is discussed elsewhere.[65,66]

The Fe_3O_4 nanocrystals were photo-excited with a 780 nm pump pulse exciting the intervalance charge transfer transition between Fe^{3+} and Fe^{2+} ions. This leads to instantaneous demagnetization in the nanocrystals as evident from decrease in Faraday rotation. The magnetization recovered in two distinct time scales. Although the origin of fast (~ 10ps) recovery component is not very clear, the slower recovery component, having $\sim 10^2$ ps timescale was assigned to spin-lattice relaxation.7 The spin-lattice relaxation rate can be altered by changing either spin-orbit coupling (and) or vibronic coupling. Due to the lack of ligand co-ordination, the surface Fe atoms experience weaker ligand field compared to the interior which result in stronger spin-orbit coupling on the surface of the nanocrystals. Therefore, the surface spin-orbit coupling which has a larger contribution in smaller nanocrystals (as the surface to volume ratio strongly increases with decreasing size) results in faster recovery of magnetism in smaller

nanocrystals. Another way to modify the surface composition and surface ligand field is to modify the surfactant and solvent environment around the nanocrystals. The surfactant molecules bound to the nanocrystals surface Fe atoms can play important role by providing different degree of co-ordination at the surface. Salafranca et. al. have shown that oleic acid on Fe_3O_4 surface can provide bulk like environment by coordinating through carboxylate group and restore the magnetism on the surface. Furthermore, Vestal et. al. have shown changing the crystal field on the surface through changing the surfactants leads to change in coercivity in $MnFe_2O_4$ nanocrystals. The solvent molecules, if they are close enough to the surface can also induce the same change as the surface passivating surfactants. Therefore, we were interested in studying the effect of surrounding surfactant and solvent media on spin-lattice relaxation dynamics of photoexcited Fe_3O_4 nanocrystals.

CHAPTER III

EXPERIMENTAL PROCEDURES*

3.1 Synthesis and Characterization of Nanocrystals

3.1.1 Synthesis of Mn-doped CdS/ZnS Nanocrystals

Mn-doped CdS/ZnS nanocrystals were synthesized using doping and layer by layer coating methods which are depicted in figure 3.1 for doping in interface between CdS and ZnS.[32,67] Initially, CdS core was synthesized using a previously reported method.[17] In brief, 0.2 M Cd solution was prepared by dissolving 0.126 gm cadmium oxide in a mixture of 12 mL1-octadecene (ODE) and 2.02 gm oleic acid at 250°C under nitrogen atmosphere.

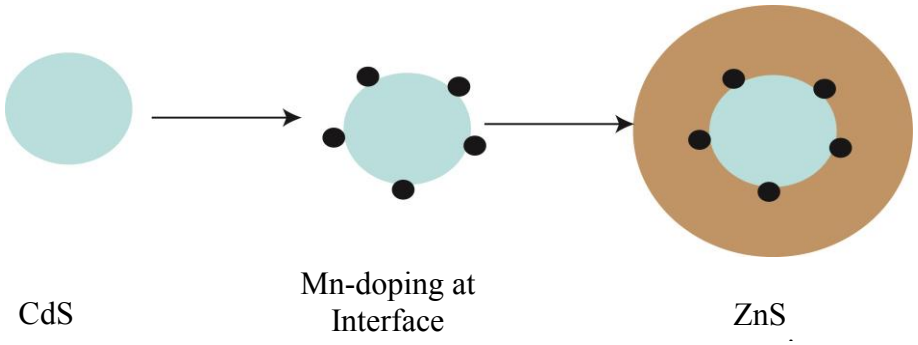

Figure 3.1 Schematic of Mn-doping and layer by layer ZnS coating to synthesize interfacial Mn-doped CdS/ZnS.

---

* Reprinted in part with permission from Maiti, Sourav; Chen, Hsiang-Yun; Chen, Tai-Yen; Hsia, Chih-Hao; Son, Dong Hee. Effect of Surfactant and Solvent on Spin–Lattice Relaxation Dynamics of Magnetic Nanocrystals**.** *J. Phys. Chem. B* **2012,** *117* (16), 4399-4405. Copyright 2012 by the American Chemical Society.

Into this hot solution 0.2 M sulfur in solution was injected. Immediately after injection the temperature was brought down to 240°C. The CdS nanocrytals started to grow and the size of the nanocrytals was monitored using UV-Vis absorption spectra. When the absorption of the nanocrystals reached 425 nm (core diameter 3.6 nm) the reaction mixture was cooled down to room temperature. The nanocrystals were precipitated with acetone and dissolved in toluene. The nanocrystals were precipitated twice from toluene with methanol to remove excess starting materials and surfactants.

For Mn-doped nanocrystals two different doping locations were chosen in this study. To synthesize interfacial Mn-doped CdS/ZnS nanocrystals Mn was doped at the CdS surface. Manganese diethyldithiocarbamate was dissolved in oleyl amine (OAm) and was added to CdS nanocrystal solution in ODE at 220 °C. The mixture was heated for 20 minutes and then cooled to room temperature. The nanocrystals were precipitated with acetone. Excess reactants and surfactants were removed by dissolving the nanocrystals in toluene and precipitating with methanol, same as the CdS nanocrystals. On the top of these Mn-doped CdS nanocrystals ZnS shell was grown. For interfacial Mn-doped nanocrystals six layers of ZnS shell (each layer is 0.6 nm) were grown by heating the nanocrystal solution in ODE and OAm to 220°C and then adding sulfur solution (in ODE) and zinc stearate solution (in ODE and octylamine) alternatively with a 10 minutes interval between subsequent additions. At the last layer of ZnS, excess zinc stearate was added to make the surface Cd rich which ensures high quantum yield of the nanocrystals. Second layer Mn-doped nanocrystals were also synthesized where two layers of ZnS were coated and then Mn was doped followed by coating four more layers

of ZnS. Two layers of ZnS were coated in the CdS core as discussed. Mn was doped at the second layer by adding OAm solution of manganese acetate to CdS/ZnS nanocrytals in ODE and OAm at 260°C. After 20 minutes the mixture was cooled and cleaned as CdS nanocrytals. Then, four layers of ZnS were added and nanocrystals were cleaned as described for the interfacial doped nanocrystals.

3.1.2 Synthesis of Iron Oxide (Fe_3O_4) Nanocrystals and Surfactant Exchange

Spherical Fe_3O_4 nanocrystals (diameter = 5.3-7.5 nm) were prepared following the procedure reported earlier.[68] The surface of the nanocrystals was passivated with several different surfactants having different head and tail groups to lender solubility in various polar and nonpolar solvents and imposes varying degree of ligand field on the nanocrystal surface. Initially, Fe_3O_4 nanocrystals were synthesized and then separate surfactant exchange reactions were performed to change the surfactants on the nanocrystal surface. In brief, Fe_3O_4 nanocrystals were synthesized by heating iron (III) acetylacetonate with a mixture of oleic acid, oleylamine and 1,2-dodecandiol using benzyl ether as the solvent under nitrogen atmosphere. Different particle size was achieved by varying the reaction temperature and reaction time. The resulting nanocrystals were precipitated with ethanol and redispersed in hexane multiple times to remove the excess surfactant.

Fe_3O_4 nanocrystals that are dispersed in polar solvents were prepared by the surfactant exchange process. The initially prepared Fe_3O_4 nanocrystals (7.5 nm) were dissolved in hexane (8.5 μM, 20 mL). The solution (4 mL) was mixed with hexane (10

mL), toluene (10 mL), methanol (10 mL) and water (2 mL) to form a bi-phasic mixture. 0.4 mL of 0.06 M methanolic solution of tetramethylammonium hydroxide (TMAH) was further added to the mixture to initiate the phase transfer. Upon gentle agitation in a separating funnel, the nanocrystals transferred from nonpolar to polar phase as a result of the surfactant exchange. Methanol was evaporated under nitrogen flow from the recovered polar phase and the TMAH-passivated Fe_3O_4 nanocrystals were precipitated with acetone to remove the access TMAH. The precipitated Fe_3O_4 nanocrystals were dried with nitrogen before dispersing in the required polar solvents. In order to prevent the partial oxidation of the nanocrystal to Fe_2O_3 phase during the process of surfactant exchange and rinsing, the exposure of the nanocrystals to atmospheric oxygen was minimized. TMAH-passivated Fe_3O_4 nanocrystals were used to prepare the nanocrystals passivated with different non-polar surfactant molecules. For instance, to prepare the nanocrystals passivated with oleic acid functionalized surfactants, excess amount of oleic acid in hexane was mixed with the TMAH-passivated nanocrystals dispersed in methanol. The exchange of surfactant from TMAH to oleic acid results in the transfer of the nanocrystals from polar phase back to non-polar phase. After the completion of the phase transfer, the nanocrystals in hexane were precipitated and rinsed with ethanol to remove the excess surfactant. During the surfactant exchange process, potential partial oxidation of the surface was checked by measuring the absorption at near infrared that correlated with the degree of oxidation. When partial oxidation occurs on the surface, gentle heating of the nanocrystal solution in octadecene at 200 °C under nitrogen atmosphere with small amount of oleic acid restored Fe_3O_4 back to the initial state.

The nanocrystals with long chain alcohol surfactants were also prepared from TMAH-passivated nanocrystals in a similar method. Excess 4-(n-octyloxy)phenol (or octadecanol) was added to a methanolic dispersion of TMAH-passivated nanocrystals. The methanol was removed under vacuum and the iron oxide nanocrystals in the solution were reduced at 200°C under nitrogen atmosphere for an hour. The alcohol-passivated nanocrystals were dissolved in hexane and precipitated with ethanol to remove the excess surfactant. The nanocrystals having different non-polar surfactants were dispersed in 1-octadecene to measure the transient Faraday rotation and transient absorption. The structure of the four surfactants used is shown in figure 3.2.

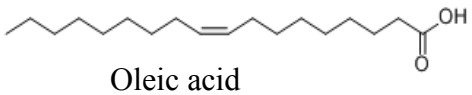

Oleic acid

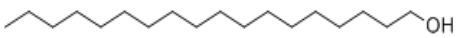

Octadecanol

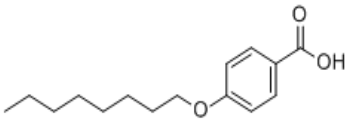

4-(n-octyloxy benzoic acid)

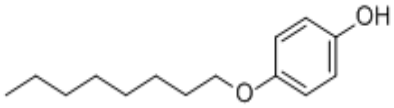

4-(n-octyloxy phenol)

Figure 3.2 Structure of the surfactants used to elucidate the effect of varying surfactant on magnetization dynamics of Fe_3O_4.

The size and shape of the nanocrystals were confirmed with transmission electron micrograph (TEM). The TEM of 7.5 nm nanocrytals is shown in Figure 3.3 (a).

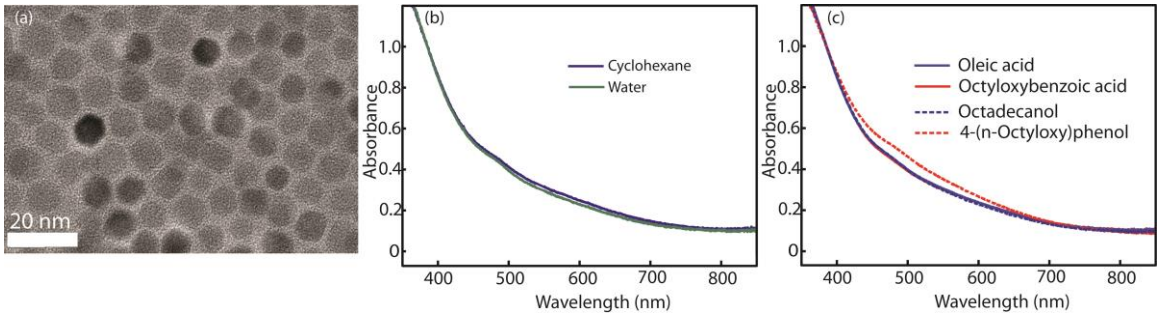

Figure 3.3 (a) TEM image of 7.5 nm Fe_3O_4 nanocrystals. UV-Vis absorption spectra of Fe_3O_4 nanocrystals (b) before and after TMAH-exchange dispersed in cyclohexane and water, respectively (diameter = 7.5 nm), (c) with different surfactants in 1-octadecene after further surfactant exchange from TMAH-passivated nanocrystals (diameter = 5.3 nm).

Figure 3.3 (b) shows the UV-Vis absorption spectra of Fe_3O_4 nanocrystals dispersed in cyclohexane before surfactant exchange and TMAH-passivated nanocrystals dispersed in water. The two spectra are very close even in the regions longer than 600 nm that is sensitive to the partial oxidation. In 3.3 (c), the UV-Vis absorption spectra of the nanocrystals having different surfactants prepared from the TMAH-passivated nanocrystals and dispersed in 1-octadecene are shown. Similarity of the UV-Vis spectra longer than 600 nm indicates that the nanocrystals used in this study have the nearly identical degree of oxidation. Also, figure 3.4 compares the TEM image before and after TMAH exchange to show the similar nanocrystal size and absence of aggregation during the exchange.

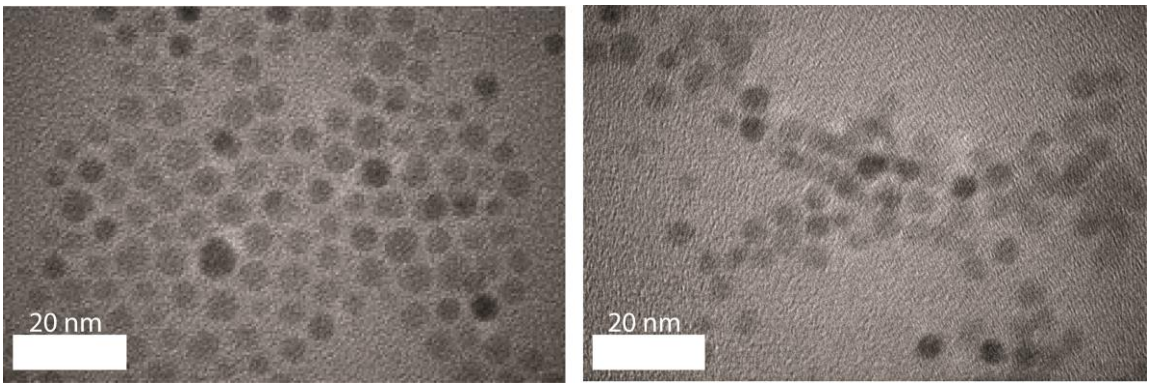

Figure 3.4 Typical TEM images of (a) as synthesized and (b) TMAH-passivated Fe_3O_4 nanocrystals.

3.2 Experimental Techniques

3.2.1 Transient Absorption Measurement on Mn-doped CdS/ZnS Nanocrystals

For the pump-probe transient absorption the nanocrytals were excited at 395 nm pulse (pulse width 100fs) with a repetition rate of 3 KHz generated from the frequency doubling of 780 nm pump in β-barium borate crystal. The 780 nm laser pulse was from a Ti:sapphire laser which was excited through a Nd:YVO_4 laser and amplified using a Nd:YLF laser. The nanocrystals were probed at the band-edge at 420 nm. The probe beam was selected from a white light continuum generated on a 1 mm thick CaF_2 crystal by the 780 nm laser. The CaF_2 crystal was moved continuously to prevent the crystal damage. The nanocrystal samples were dissolved in spectroscopic grade toluene (concentration 6.4 μM) and circulated through a 1 mm thick cuvette with a flow rate of 1 m/s. As the Mn lifetime is ms, the flow rate was fast enough so that each pulse excites fresh Mn-doped nanocrystals in the cuvette. The pump beam size was 300 μM and probe

beam size was 30 μM. The pump beam intensity was low enough not to have more than 1 exciton in the nanocrystals to avoid complications arising from biexcitonic effects. A sketch of the optical setup is shown in figure 3.5.

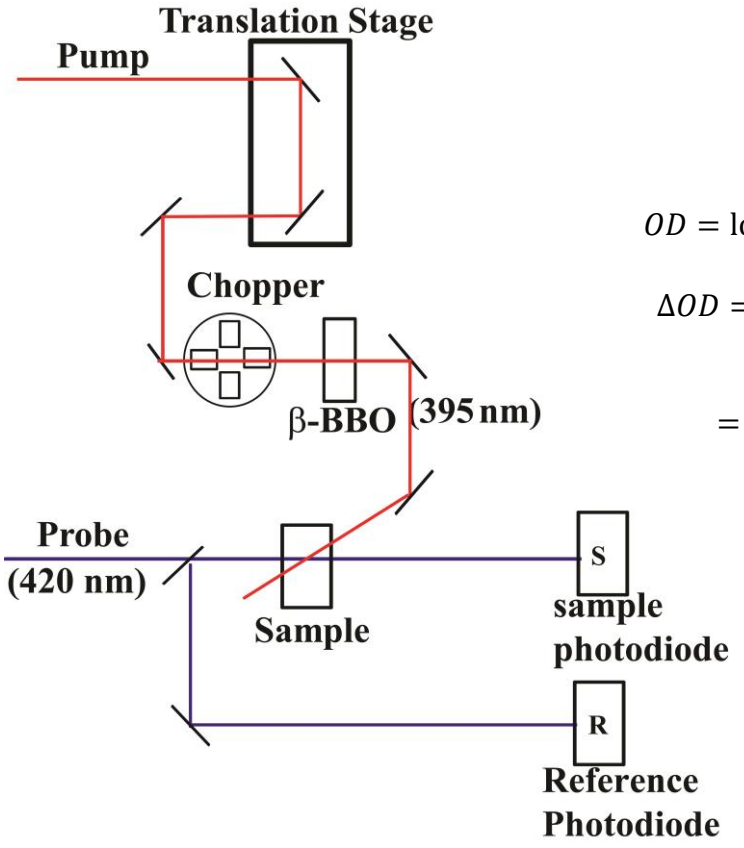

$$OD = \log(\frac{I_{reference}}{I_{sample}})$$

$$\Delta OD = OD_{pump\ on} - OD_{pump\ off}$$

$$= \log\left(\frac{I_{refrence}^{pump\ on}}{I_{sample}^{pump\ on}}\right) + \log(\frac{I_{reference}^{pump\ off}}{I_{sample}^{pump\ off}})$$

Figure 3.5 Schematic of transient absorption measurement and relevant equations.

3.2.2 Determination of Mn-Quantum Yield and Mn-Lifetime of Mn-doped CdS/ZnS

The Mn-quantum yield was determined using previously reported procedure.[32] The quantum yield measurements have about 5% error. To determine the effect of octanethiol on the Mn-photoluminescence, required amount of octanethiol was added to a solution of nanocrystals in toluene (~0.4 μM). After addition of octanethiol, about 30 min was waited to allow the thiol to mix properly. Nanocrystals were excited at 405 nm with a *cw* laser and the spectra were detected with an ocean optics spectrometer (QE65Pro).

To measure the Mn-lifetime in Mn-doped CdS/ZnS nanocrystals the nanocrystals dispersed in toluene were excited with a nitrogen laser (pulse width <3ns) at 337 nm. The Mn-emission was collected in photomultiplier tube and recorded in a digital oscilloscope. From bi-exponential fitting of the time dependent Mn-emission intensity, the average Mn-lifetime was calculated through equation 3.1, where a_1 and a_2 are the pre-exponential factors and t_1 and t_2 are the time constants.

$$\tau_{Mn} = \frac{a_1 t_1^2 + a_2 t_2^2}{a_1 + a_2} \qquad (3.1)$$

3.2.3 Transient Faraday Rotation and Transient Absorption Measurements for Fe_3O_4 nanocrystals

In order to measure the spin-lattice relaxation rate, pump-probe transient Faraday rotation was employed to record the time-dependent magnetization, M(t), following the optically-induced partial demagnetization. The details of the measurements are described elsewhere.[53,54] Briefly, 780 nm pump pulse (50 fs pulse width) from an amplified titanium-sapphire laser excited intervalence charge transfer transition in the iron oxide nanocrystals, which rapidly induces the demagnetization. The recovery of the magnetization via spin-lattice relaxation was monitored with 635 nm probe pulse derived from white light continuum generated in a sapphire crystal. The time-dependent magnetization of the nanocrystal sample was measured in Faraday geometry with a pair of permanent magnet applying 0.35 T (H) of magnetic field at the sample location. The polarization direction of the incident probe beam was defined by a Glan polarizer placed in front of sample. The probe beam passing through the sample was split into two orthogonal polarization components using a Wollaston prism set at 45° angles with respect to the polarization direction of the probe beam. A pair of balanced photodiodes measured the difference in intensities between the two orthogonal components of the polarized light, which is proportional to Faraday rotation angle $\theta(t)$. The fractional change in Faraday rotation between with and without pump, $\Delta\theta(t)/\theta_0$, represents the fractional changes in magnetization $\Delta M(t)/M_{0,}$ where θ_0 and M_0 are the Faraday rotation and magnetization without pump, respectively. To remove the non-magnetic

contribution to $\Delta\theta(t)/\theta_0$ signal, the difference between the two sets of data taken with parallel and antiparallel magnetic field to the probe beam direction was used to measure $\Delta\theta(t)/\theta_0$. The values of θ_0 for the samples of given nanocrystal concentration were determined from the slope of the Faraday rotation vs. nanocrystal concentration measured using a separate setup as described in the earlier report.[69] The relative values of θ_0 of different Fe_3O_4 nanocrystal samples with respect to the oleic acid-passivated nanocrystal dispersed in cyclohexane are summarized in Table 3.1. In order to avoid the potential complication from the lattice heating by the pump, all the measurements were made at low excitation intensity ranges that does not affect the dynamics of $\Delta\theta(t)/\theta_0$.[70] In figure 3.6 the optical setup is shown.

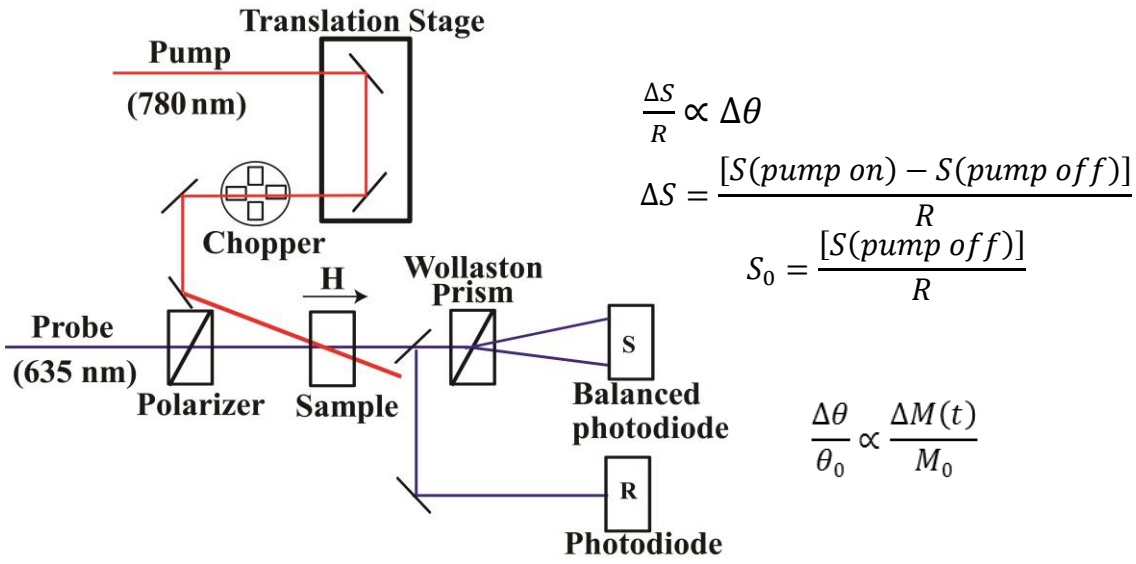

Figure 3.6 Schematic of transient Faraday rotation measurement.

Transient absorption of the nanocrystal samples were measured simultaneously at the same pump (780 nm) and probe (635 nm) wavelengths for the transient Faraday rotation. The optical setup is same as shown in figure 3.5 without the BBO crystal as 780 pump beam was used. The comparison of the transient absorption with and without the external magnetic field indicated that transient absorption is completely insensitive to the external magnetic field applied in this study. For all the comparisons, same pump fluence and sample concentrations were used to create the same level of excitation in the nanocrystals. The concentration of the nanocrystal samples was kept at ~10 μM for 5.3 nm nanocrystals and ~3 μM for 7.5 nm nanocrystals to avoid interparticle dipolar interaction that can change the dynamics.[71] For both transient Faraday rotation and transient absorption measurements, the sample solutions of nanocrystals were constantly circulated through a flat jet nozzle to avoid any spurious thermal effect from the repeated excitation of the same sample area.

Surfactant	θ_r
oleic acid	1.0
4-(octyloxy)benzoic acid	1.0
4-(n-octyloxy)phenol	0.69
octadecanol	0.69

Table 3.1 Comparison of the relative static Faraday rotation (θ_r) of Fe_3O_4 nanocrystals with different surfactants (diameter = 5.3 nm) with respect to the oleic acid-passivated nanocrystals. The uncertainty of θ_r is <5 %.

CHAPTER IV

EFFECT OF OCTANETHIOL ON ENERGY TRANSFER DYNAMICS IN Mn-DOPED CdS/ZnS CORE/SHELL NANOCRYSTALS

4.1 Introduction

Semiconducting nanocrystals doped with transition metal ions have attracted tremendous attention in recent years due to important optical and magnetic properties that arise due to dopant-exciton interaction.[20-23,72,73] In this context, Mn ions doped in II-VI semiconducting host have been widely studied due to interesting properties applicable in luminescence studies and spintronics. Mn-doped nanocrystals exhibit high Mn-emission quantum yield due to fast exciton-Mn energy transfer which competes with other non-radiative processes.[20,73,74] Energy transfer is possible only when Mn excited states reside within the bandgap of the semiconducting host. The energy transfer rate depends on the exciton-Mn wavefunction overlap.[20] Here, we have explored the effect of hole trapping surfactant, octanethiol on the exciton-Mn energy transfer dynamics in Mn-doped CdS/ZnS nanocrystals through transient absorption measurements. Our findings reveal that although octanethiol traps more hole, addition of octanethiol increases Mn-luminescence quantum yield due to energy transfer from thiol traps to Mn.

As discussed earlier surfactants play an important role in determining exciton dynamics in semiconducting nanocrystals. The role of surface ligands on excitonic photoluminescence and exciton relaxation dynamics is well-documented for semiconducting nanocrystals. Surfactants are known to change the excitonic transition

energy and extinction coefficient, emission intensity and lifetime of the exciton.[75-77] Also, some organic surfactants are known to couple strongly with the exciton to change quantum confinement effects in the nanocrystal.[78,79] Depending on the energetics of the surfactant and exciton, a surfactant can either be electron traps or hole traps. Thiols are one of the well-known hole-trapping surfactants which can change the exciton luminescence intensity and wavelength.[75,78] They are also one of the important surface passivating ligands as thiol passivation makes the nanocrystals to be water soluble, which is important in the case of biological applications.[80] However, for thiols to act as hole quenchers the acceptor orbital of thiols (highest occupied molecular orbital, HOMO) should be higher in energy than the valence band-edge of the nanocrystal. Therefore, thiols are excellent hole trapping ligands for CdS or CdSe nanocrystals where the HOMO of thiols remain higher in energy than the valance band of the nanocrystal to accept the hole. Thiols trap the hole preventing exciton recombination and consequently decreasing the exciton emission intensity. Therefore, hole trapping thiols decrease exciton emission intensity in CdSe or CdS nanocrystals even in the core/shell structures such as CdSe/ZnS.[75,81-86] Thiols generally bind as thiolates on the nanocrystal surface.[87] Therefore, thiol exchange with proper thiol concentration and using mild basic conditions can retain the exciton quantum yield to produce highly luminescent water soluble CdSe/ZnS core/shell nanocrystals.[87,88] However, in the case of CdTe nanocrystals where thiols have energetically unfavorable HOMO, thiols cannot quench the exciton emission. In CdTe nanocrystals thiols tend to increase the exciton emission through better surface passivation.[75,89,90] Jeong et. al. reported at low concentration of β-

mercaptoethanol enhances the photoluminescence of polymer coated CdSe/ZnS nanocrystals whereas high concentration of thiol quench it. Thiolate was identified as the effective species responsible for the effects. At low concentration, thiol passivates electron traps enhancing photoluminescence whereas at high concentrations it introduces new hole traps to decrease the exciton photoluminescence.[91] Moreover, the effect of thiol on exciton relaxation dynamics was investigated using transient absorption measurements. Hole trapping timescale generally is in the order of few ps for CdSe nanocrystals as reported by Burda et.al. using 4-aminothiophenol and McArthur et. al. using octanethiol as the hole quenchers.[37,61]

In Mn-doped nanocrytals the exciton emission is quenched through fast exciton-Mn energy transfer. Interestingly, it is reported that in Mn-doped ZnSe nanocrystals thiols can increase the Mn-emission intensity in contrary to undoped nanocrystals.[80] This was qualitatively explained through the competition between exciton-Mn energy transfer and hole trapping. In doped quantum dots the hole trapping has to compete with the exciton-Mn energy transfer process. For thin ZnSe shell hole trapping was faster than energy transfer which quenches the Mn-emission. For thicker ZnSe shell, the hole gets spatially separated from the surface decreasing the hole trapping rate. Therefore, the extent of exciton-Mn energy transfer increases which increases Mn-emission. Although, the observation was interesting and was explained in qualitative grounds no detailed information about the completion between the hole trapping and exciton-Mn energy transfer was obtained quantitatively. Increase in photoluminescence is also observed for Mn-doped ZnS nanocrystals although the explanation of decrease in hole transfer

efficiency with thiols is highly ambiguous.[92] Recently, Sarkar et.al. have reported that using thiols the dopant-luminescence can be retrieved with higher emission intensity from old nanocrystals for Cu and Mn-doped ZnSe. Thiols are believed to prevent surface oxidation and act as a reducing agent.[93] However, these explanations are also very qualitative.

Our group has recently studied exciton dynamics in Mn-doped CdS/ZnS core/shell nanocrystals where the exciton-Mn energy transfer rate was accurately obtained for different location and concentration of Mn through transient absorption measurements.[32,52] It was found that due to increased exciton-Mn wavefunction overlap energy transfer rate increases when Mn is doped closer to the interface with highest energy transfer rate for interfacial doped nanocrystals. Also, hole trapping was found to be the major competing process in the nanocrystals which prevents energy transfer and decreases Mn-emission. The branching ratio between hole trapping and energy transfer was obtained from transient absorption measurements and was successfully correlated with Mn-emission intensity and lifetime.[32] Knowing all the detailed information about intrinsic hole trapping rate and energy transfer rate, we extended our study to observe the effect of a hole trapping ligand, octanethiol on Mn-emision and exciton dynamics through steady state and time resolved measurements.

In this study, the effect of a hole trapping ligand octanethiol on the exciton-Mn energy transfer dynamics and Mn emission was investigated in Mn-doped CdS/ZnS nanocrystals. Undoped CdS/ZnS nanocrystal was also, synthesized as a reference. The exciton emission in undoped nanocrystals gets almost completely quenched in the

presence of octanethiol. The effect of octanethiol on the Mn-luminescence was quite interesting. The luminescence tends to increase for Mn-doped nanocrystals in contrast to undoped nanocrystals and the extent of increase depends on the Mn concentration in the nanocrystal. Transient absorption measurements revealed that octanethiol leads to hole quenching which should decrease the extent of energy transfer and Mn-emission intensity. This was explained though energy transfer to Mn from hole traps created by octanethiol which increases the Mn-emission intensity.

4.2 Results and Discussion

Two different Mn-doped CdS/ZnS nanocrystals, one with interfacial Mn-doping and the other with Mn-doped at the second layer of ZnS were prepared along with the undoped counterpart. The CdS core has a diameter of 3.6 nm and each layer of ZnS is 0.6 nm. UV-Vis and emission spectra of the three (undoped, interfacial and second layer Mn-doped) nanocrystals are shown in figure 4.1. Representative TEM images of Mn-doped nanocrystals are shown in appendix (figure A2). The similarity of the absorption spectra especially in the higher wavelength region implies that the nanocrystals are structurally similar. The undoped nanocrystal has exciton emission centered around 430 nm. In the Mn-doped nanocrystals, the exciton emission is quenched due to fast exciton-Mn energy transfer and they exhibit Mn-emission around 620 nm. The Mn emission is centered on 622 nm for interfacial doped nanocrystal and 613 nm for second layer doped nanocrystal. The blue shift in the emission maxima for second layer doped nanocrystal is consistent with decrease in local lattice strain as the Mn-is doped away from the

interface.[94,95] Mn $^4T_1$ to $^6A_1$ spin forbidden transition energy is the difference between the pairing energy (P.E.) and ligand field stabilization energy (P.E.- Δ). Decrease in the local lattice strain leads to increase in the Mn-S bond length decreasing the crystal field stabilization energy (Δ). As Δ decreases, the emission energy increases and the emission maximum blue shifts for second layer Mn-doped nanocrystal.

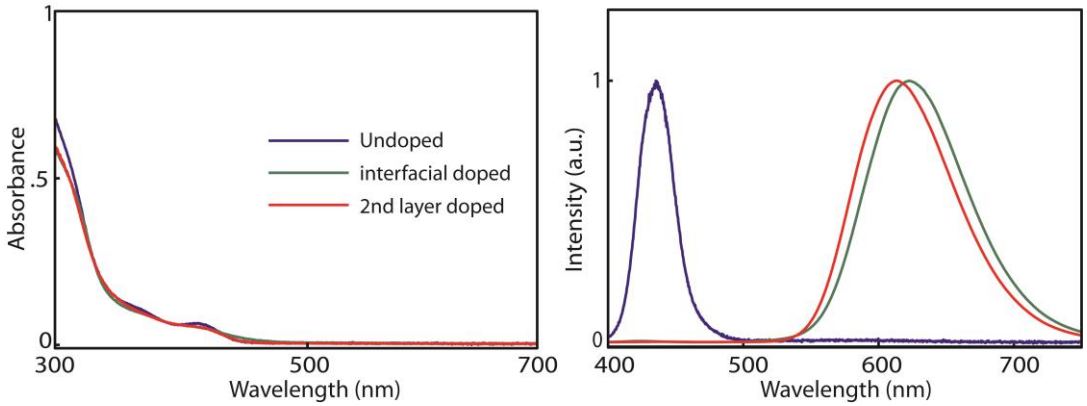

Figure 4.1 (a) Absorption and (b) emission spectra of undoped and Mn-doped CdS/ZnS nanocrystals.

Mn-emission quantum yield and Mn-lifetime nanocrystals are determined as discussed in chapter 2 and shown in table 4.1. The average number of Mn in Mn-doped nanocrystals are determined through inductively coupled plasma mass spectrometry (ICP-MS), is also shown in table 4.1. To compare the effects of shell thickness on exciton dynamics in Mn-doped nanocrystals upon adding octanethiol, a thin shell sample was also synthesized (CdS/ZnS/5.3Mn/1.5 ZnS).

Sample	<Mn>	Φ_{Mn}	τ_{Mn}	φ_{Mn}	$\tau_{Mn}/\tau_{Mn,r}$
CdS/6ZnS Mn at the interface	18	0.60	4.2	0.66	0.67
CdS/6ZnS Mn at the 2nd layer	15	0.72	4.5	0.84	0.71

Table 4.1 Mn concentration (<Mn>), Mn-PL quantum yield ($\mathbf{\Phi_{Mn}}$), Mn-lifetime (τ_{Mn}), Mn-radiative quantum yield (φ_{Mn}, calculated from equation 4.7) and ratio of Mn-lifetime to Mn-radiative lifetime (assuming Mn-radiative lifetime is 6.3 ms) in Mn-doped CdS/ZnS nanocrystals.

4.2.1 Transient Absorption Measurements with Octanethiol on Mn-doped CdS/ZnS Nanocrystals

Transient absorption measurements were performed on both undoped and doped nanocrystals in the presence of octanethiol. The nanocrystals were excited at 395 nm and the change in absorption (ΔOD) was measured probing at the band-edge at 420 nm. The pump excites the electrons from valence band to the conduction band making the conduction band-edge partially filled, therefore if probed at the band-edge the probability of exciton formation is decreased and the ΔOD becomes negative. Over time the electron relaxes which is manifested in the recovery of ΔOD, known as bleach recovery. This bleach recovery at the band-edge mainly represents the electron dynamics.[7,36,57-60] Figure 4.2 shows the bleach recovery of undoped CdS/ZnS nanocrystals in presence of octanethiol. In undoped nanocrystals the bleach recovery is

mainly due to exciton recombination and charge carrier trapping which is depicted in figure 4.3. Addition of hole trapping surfactants such as octanethiol slows down the bleach recovery as it traps more holes preventing the exciton recombination process. Slowing down of the bleach recovery with hole trapping surfactants is consistent with earlier studies. The bleach recovery from undoped nanocrystals was fitted mono-exponentially with ~1 ns time scale.

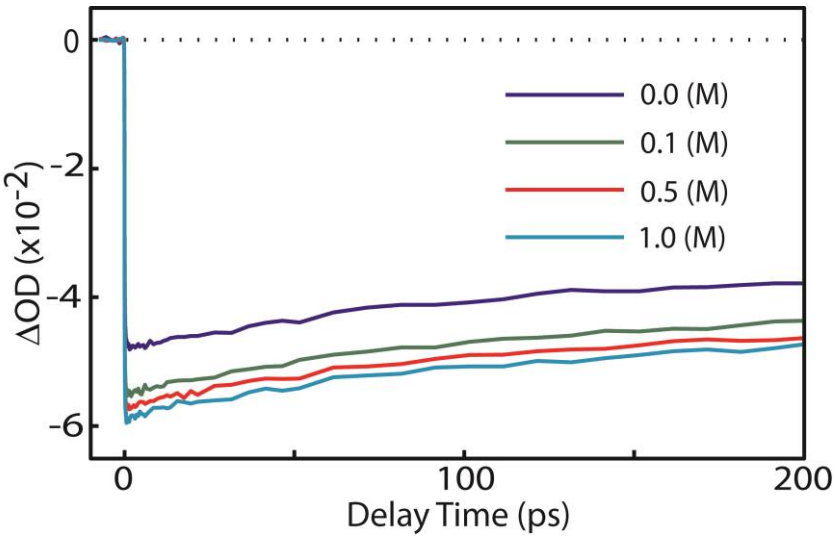

Figure 4.2 Bleach recovery dynamics of undoped CdS/ZnS nanocrystal with increasing amount of octanethiol (pump at 395 nm, probe at 420 nm).

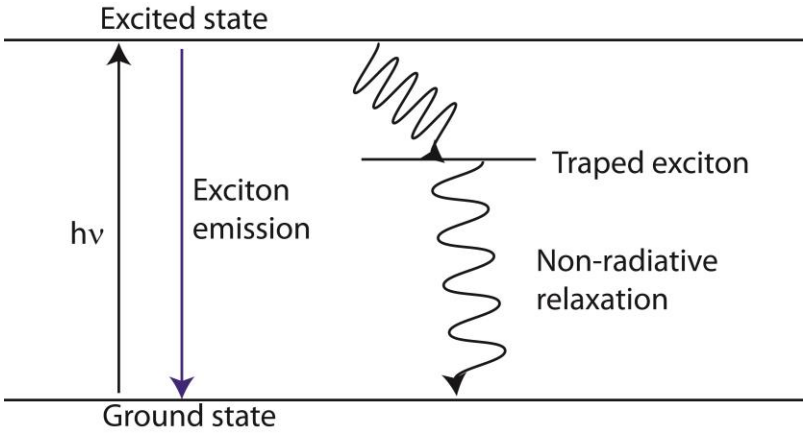

Figure 4.3 Schematic of exciton relaxation processes in undoped CdS/ZnS nanocrystals.

Figure 4.4 shows the bleach recovery dynamics in presence of increasing amount of octanethiol for all the Mn-doped nanocrystals used in this study. First, the effect of Mn-doping on the exciton dynamics will be discussed in brief in accordance with our earlier studies. Then the effect of octanethiol will be elucidated. Due to additional contribution from exciton-Mn energy transfer, the bleach recovery in Mn-doped nanocrystals is much faster. Figure 4.5 depicts the different exciton relaxation processes in Mn-doped nanocrystals.

The bleach recovery in the Mn-doped nanocrystals has a fast component due to energy transfer along with a slow component. The slow component has time scale similar to the undoped nanocrystals (~ 1ns). The origin of this slow component was assigned to hole trapping which competes with exciton-Mn energy transfer. The hole trapped nanocrystals do not have exciton-Mn energy transfer and behave as undoped nanocrystals leading to this slow component. The fast component due to exciton-Mn energy transfer is fitted to two exponentials similar to our earlier study.[32] Therefore, the

bleach recovery in doped nanocrystals is fitted with the sum of three exponential functions (equation 4.1). First two exponentials represent exciton-Mn energy transfer and the third exponential is due to hole trapped nanocrystals having a long ~ 1ns time scale. Energy transfer time scale is extracted by averaging first two exponentials as shown in equation 4.2. The efficiency of energy transfer is given by combination of $A_1$and A_2 (equation 4.3) whereas the amplitude of third exponential (A_3) represents the efficiency of hole trapping (equation 4.4). Hole trapping time (τ_{trap}) is obtained from the branching ratio between energy transfer and hole trapping (equation 4.5).

$$-\Delta OD = A_1 \exp\left(-\frac{t}{\tau_1}\right) + A_2 \exp\left(-\frac{t}{\tau_2}\right) + A_3 \exp\left(-\frac{t}{\tau_3}\right) \quad (4.1)$$

$$\tau_{ET} = \frac{(A_1\tau_1 + A_2\tau_2)}{(A_1 + A_2)} \quad (4.2)$$

$(A_1+A_2)= f_{ET}$ = efficiency of energy transfer (4.3)

$A_3 = f_{trap}$ = efficiency of hole trapping (4.4)

$$f_{trap} = \frac{k_{trap}}{k_{ET}+k_{trap}} \quad (4.5)$$

$$= \frac{\tau_{trap}^{-1}}{\tau_{ET}^{-1} + \tau_{trap}^{-1}}$$

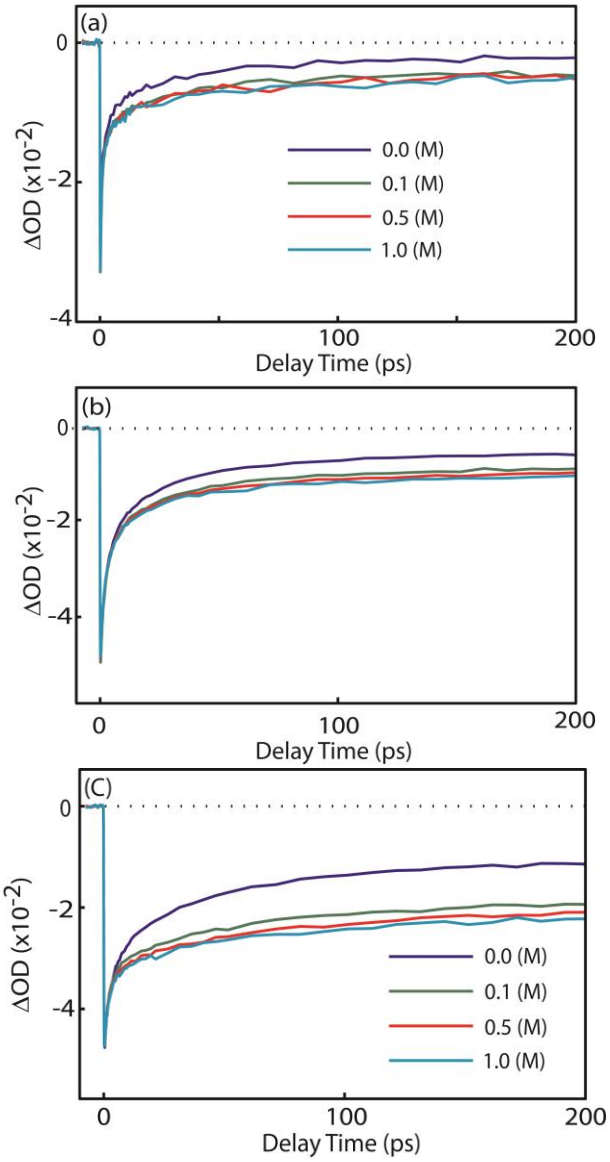

Figure 4.4 Transient absorption data for Mn-doped CdS/ZnS with increasing amount of octanethiol (pump at 395 nm and probe at 420 nm) (a) interfacial doped, (b) 2nd layer doped and (c) thin ZnS layer nanocrystal.

Addition of octanethiol has a pronounced effect on bleach recovery dynamics for Mn-doped nanocrystals. Table A1 lists all the extracted parameters for Mn-doped nanocrystals using equation 4.1 and 4.5. The addition of octanethiol has two distinct effects (Figure 4.6). First, addition of octanethiol makes the exciton-Mn energy transfer slightly faster. The addition of octanethiol possibly extends the hole wavefuntion to the surface leading to increased exciton-Mn wavefunction overlap which increases the energy transfer rate. Additionally, the amplitude of long decay component (f_{trap}: representing the hole trapping efficiency) increases with increasing octanethiol concentration. The increase of f_{trap} is consistent with the hole trapping nature of octanethiol. The hole trapping rate due to octanethiol (and thus hole trapping time, τ_{OT}) can be calculated by subtracting the combined hole trapping rate after adding octanethiol from the intrinsic hole trapping rate (equation 4.6). It was found that the hole trapping time (τ_{trap}) was much slower than the energy transfer time. The hole trapping efficiency, exciton-Mn energy transfer time, hole trapping time and hole trapping time due to octanethiol are plotted in figure 4.6 (a), (b), (c) and (d) respectively. In the interfacial doped nanocrystal the energy transfer is the fastest and gets slower in 2nd layer doped nanocrystal due to decreased exciton-Mn wavefunction overlap. The 2nd layer doped nanocrystal has higher hole trapping efficiency as the energy transfer is slower than interfacial doped nanocrystal, therefore, the competitive hole trapping process is more probable. The thin shell nanocrystal has the highest hole trapping efficiency. The exciton wavefunction extends to the surface due to thinner ZnS shell and the hole has higher probability of being trapped. Also, the energy transfer rate is slowest

in this nanocrystal making competitive hole trapping more efficient. Moreover, hole trapping due to octanethiol (represented by τ_{OT}) becomes faster as octanethiol concentration is increased. τ_{OT} decreases more rapidly in the thin shell sample as the octanethiol will trap holes more efficiently due to thin ZnS passivation.

$$k_{OT} = k_{trap}(with\ OT) - k_{trap}\,(without\ OT) \qquad \tau_{OT} = k_{OT}^{-1} \qquad (4.6)$$

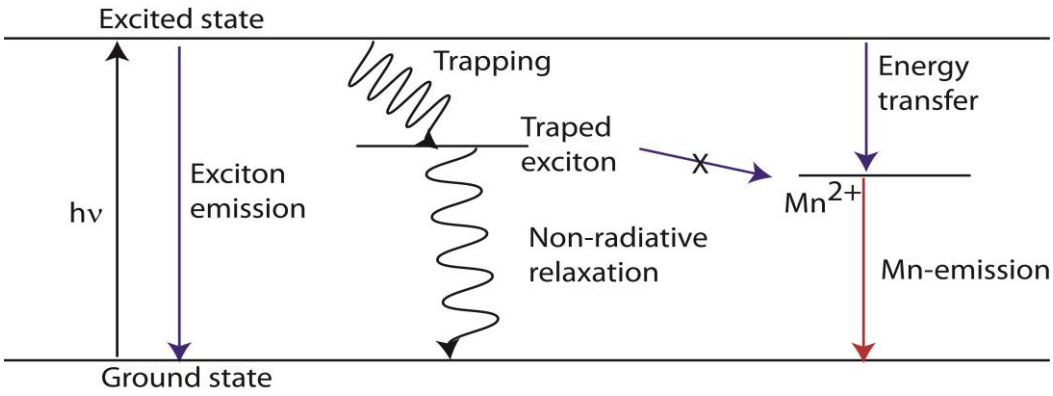

Figure 4.5 Schematic of exciton relaxation processes in Mn-doped CdS/ZnS nanocrystal.

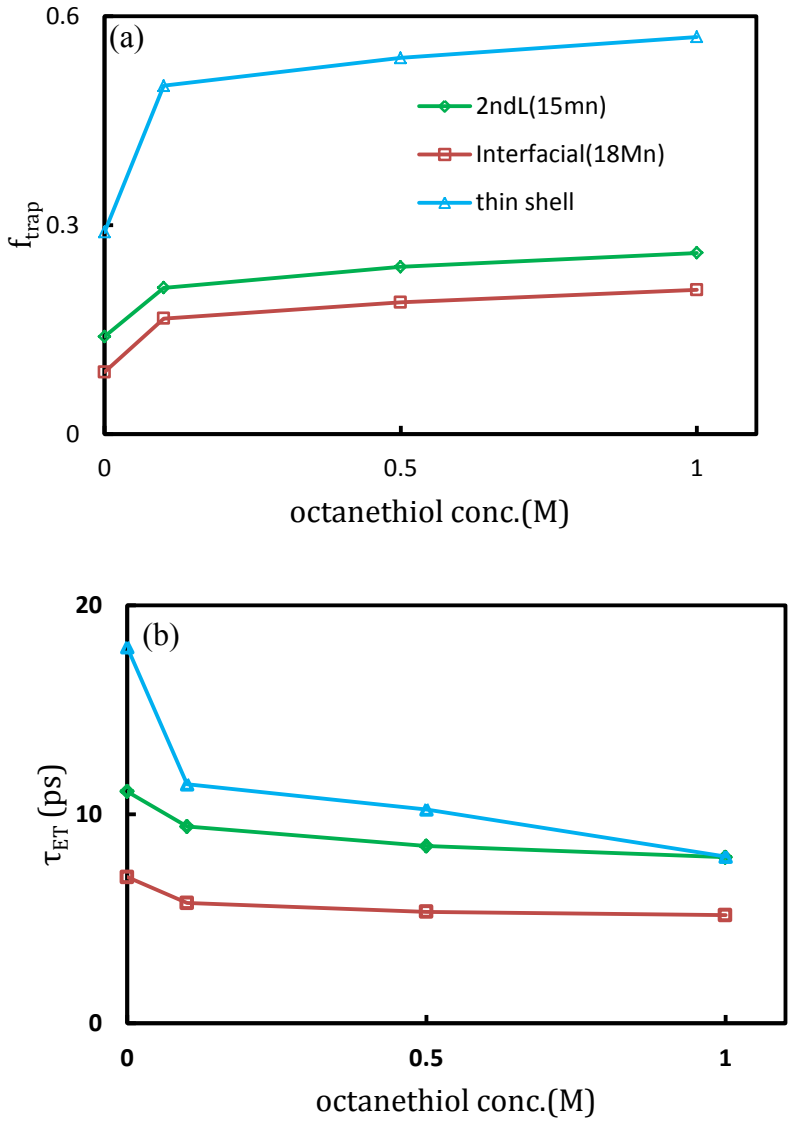

Figure 4.6 Hole trapping efficiency (f_{trap}), exciton-Mn energy transfer time (τ_{ET}), hole trapping time (τ_{trap}) and hole trapping time due to octanethiol (τ_{OT}) for Mn-doped nanocrystals; interfacial Mn-doped (□), 2nd layer Mn-doped (◇) and thin ZnS shell nanocrystal (△).

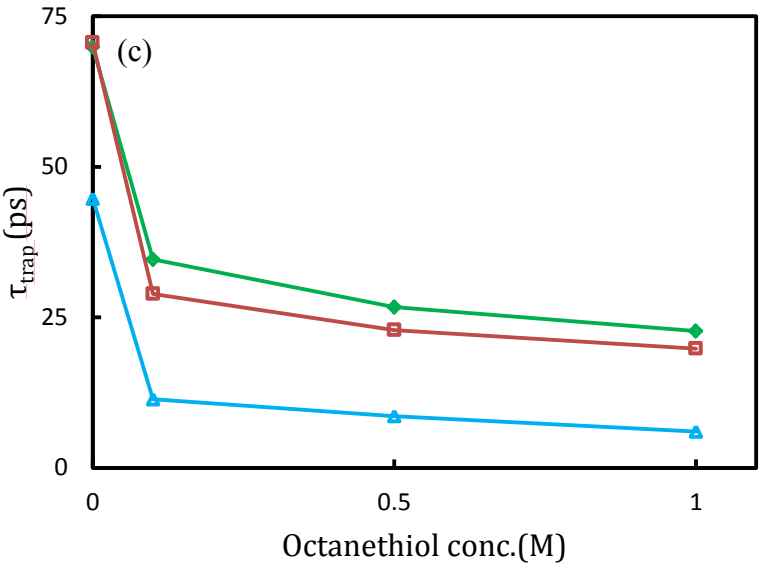

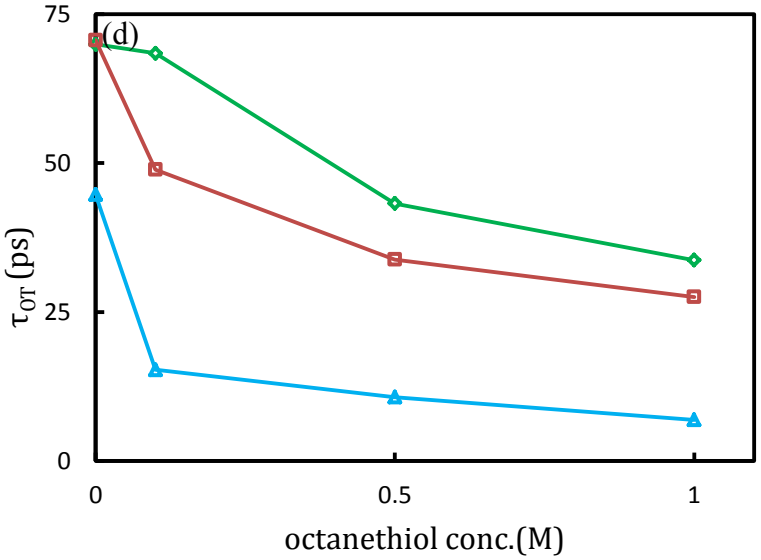

Figure 4.6 Continued.

4.2.2 Effect of Octanethiol on Mn-PL Intensity and Lifetime

Exciton luminescence in undoped CdS/ZnS nanocrystals is completely quenched after adding octanethiol. The Mn-PL intensity in the thin shell nanocrystals is also found to decrease. However, effect of octanethiol on thick ZnS passivated nanocrystals (interfacial and 2nd layer Mn-doped) is quite interesting. Mn-luminescence quantum yield ($\boldsymbol{\Phi_{Mn}}$) depends on the exciton-Mn energy transfer efficiency (f_{ET}) and radiative Mn-luminescence quantum yield (ϕ_{Mn}).

$$\boldsymbol{\Phi_{Mn}} = f_{ET} \times \phi_{Mn} \tag{4.7}$$

ϕ_{Mn} depends on the Radiative and non-radiative decay rates of Mn as shown in equation 4.8. From transient absorption measurements we have seen f_{ET} decreases with octanethiol concentration as the efficiency of hole trapping (f_{trap}) increases. The radiative Mn-luminescence quantum yield does not change on adding octanethiol as the lifetime of Mn-emission does not depend on octanethiol concentration shown in figure 4.7. Therefore, we expect a decrease in Mn-PL intensity after upon adding octanethiol as in the case for thin shell nanocrystal.

$$\phi_{Mn} = \frac{k_r}{k_r + k_{nr}} \tag{4.8}$$

$$= \frac{\tau_{Mn}}{\tau_r}$$

Surprisingly, the Mn-PL intensity is found to increase with octanethiol concentration for interfacial and 2nd layer Mn-doped nanocrystals which have thicker ZnS passivation (figure 4.8). The increase in Mn-PL is counterintuitive and cannot be explained through equation 4.7.

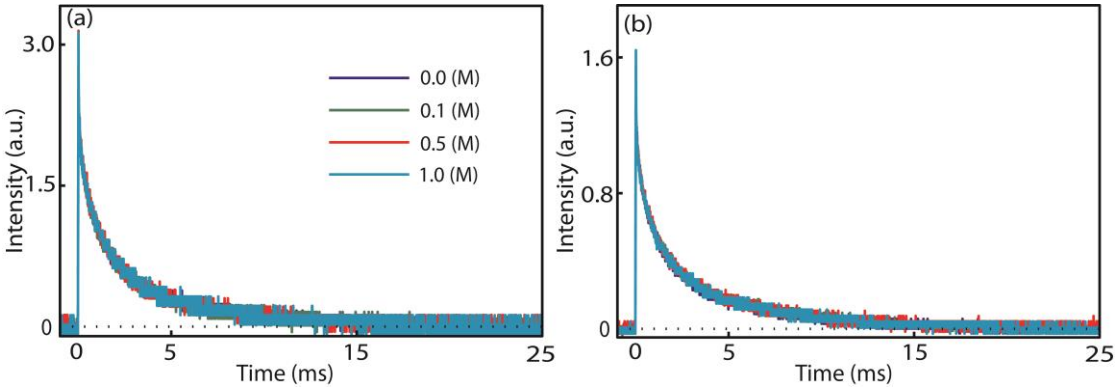

Figure 4.7 Effect of octanethiol on Mn-lifetime in Mn-doped nanocrystals (a) interfacial doped and (b) 2nd layer doped (intensity normalized to 0M octanethiol concentration).

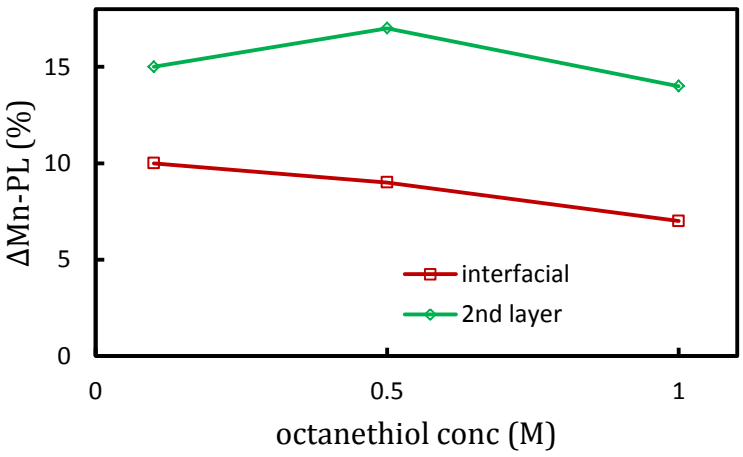

Figure 4.8 Effect of octanethiol on Mn-PL intensity in Mn-doped CdS/ZnS nanocrystals (a) interfacial doped and (b) 2nd layer doped.

Addition of octanethiol does not change the Mn-emission wavelength in these nanocrystals, as shown in the appendix figure A1.

4.2.3 Effect of Mn-Concentration on Mn-emission in the Presence of Octanethiol

Mn-emission intensity increases in the presence of octanethiol for thicker ZnS passivation. The more is the number of Mn, the more is the increase in the Mn-emission intensity for the same 6 layer ZnS thickness. For two different doping locations, with increase in Mn-concentration, the Mn-emission intensity increases more for same octanethiol concentration, this is shown in figure 4.9.

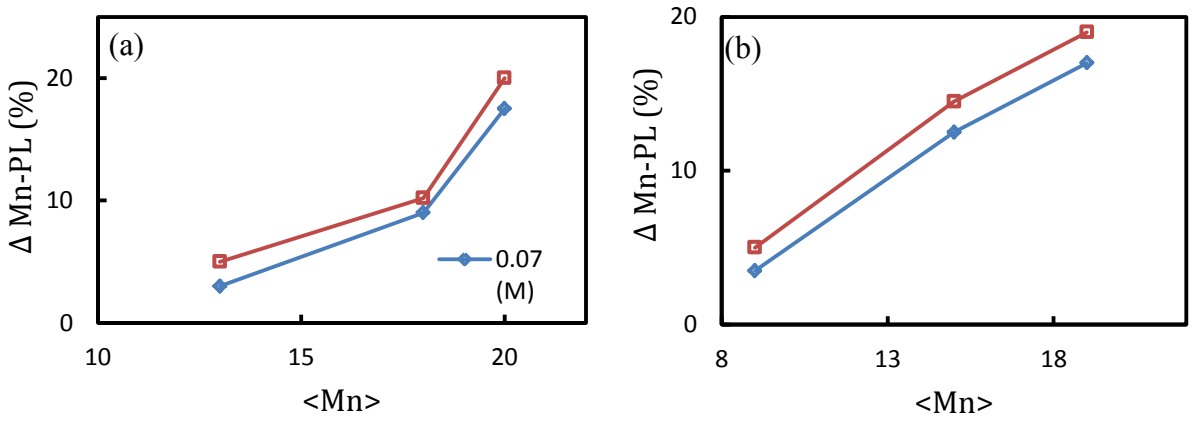

Figure 4.9 Increase in Mn-PL with two different octanethiol concentration for different Mn concentration in (a) interfacial doped and (b) 2nd layer doped CdS/ZnS.

Presence of Mn-dopants leads to fast exciton-Mn energy transfer which results in Mn-emission. After adding octanethiol, it creates additional hole traps which is

manifested in the increase of f_{trap} with increasing amount of octanethiol. As the radiative Mn-luminescence quantum yield (Φ_{Mn}) does not depend on octanethiol concentration, the increase of Mn-PL must come from an additional energy transfer from thiol hole traps to Mn which excites the Mn and increases the Mn-PL intensity. This is shown in figure 4.10. Intrinsic hole trapping is a competitive process to exciton-Mn energy transfer and this hole trapped exciton does not energy transfer back to Mn. However, exciton trapped in hole traps created by octanethiol can slowly energy transfer back to Mn to increase the Mn-luminescence intensity. Therefore we write the Mn-luminescence quantum yield ($\boldsymbol{\Phi_{Mn}}$) as equation 4.9 where we introduce an extra term f_{ET}^{OT} to account for the contribution due to energy transfer from octanethiol hole traps. The extent of this additional energy transfer depends on the number of Mn and octanethiol concentration. Therefore, with increase in Mn-doping concentration, it was found that the Mn-PL intensity increase after adding octanethiol. However, increase in Mn-PL was not very regular with increase in octanethiol concentration. The actual amount of traps created by octanethiol is not so easy to decipher. Also, the number of octanethiol actually on the surface, which will affect the number of traps created, is still under investigation. For thin ZnS passivation, Mn-PL is quenched in the presence of octanethiol. Due to thinner passivation the energy transfer rate is on the same order as the hole trapping rate and hole trapping efficiency is very high, as evident from transient absorption measurements. Therefore, the additional energy transfer may not be sufficient to circumvent the effect of hole trapping which leads to decrease in Mn-PL in the presence of octanethiol.

$$\boldsymbol{\Phi_{Mn}} = f_{ET} \times \phi_{Mn} \times f_{ET}^{OT} \qquad (4.9)$$

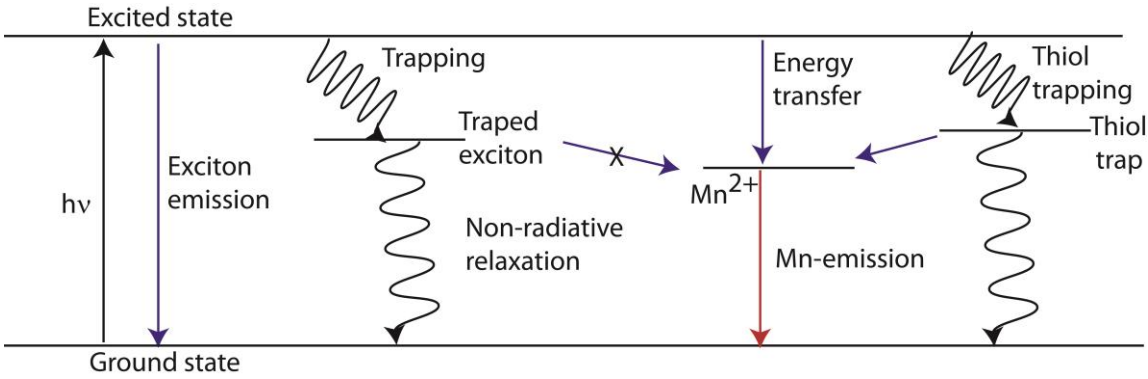

Figure 4.10 Schematics of octanethiol hole trapping.

4.3 Conclusion

Hole trapping surfactants are known to decrease exciton luminescence quantum yield in CdS or CdSe nanocrystals. However, in Mn-doped nanocrystals the exciton energy is channelized to Mn through exciton-Mn energy transfer and this leads to Mn-emission. Octanethiol being a hole trapping ligand quenches exciton emission but increases Mn-emission in CdS/ZnS nanocrystals with sufficient ZnS thickness. Transient absorption measurement reveals that octanethiol traps the hole in both doped and undoped nanocrystals, however in Mn-doped nanocrystals Mn-PL increases due to energy transfer from octanethiol trapped exciton. Through steady state and time resolved measurements, we have investigated the role of octanethiol on Mn-luninescence and exciton-Mn energy transfer dynamics which were previously unexplored.

CHAPTER V

EFFECT OF SURFACE ENVIRONMENT ON SPIN-LATTICE RELAXATION DYNAMICS OF IRON OXIDE NANOCRYSTALS*

5.1 Introduction

The effect of varying the surfactant and solvent medium on the dynamics of spin-lattice relaxation in photoexcited Fe_3O_4 nanocrystals has been investigated by measuring the time-dependent magnetization employing pump-probe transient Faraday rotation technique. The variation of the surfactants having surface-binding functional groups modified not only the static magnetization but also the dynamics of the recovery of the magnetization occurring via spin-lattice relaxation in the photoexcited Fe_3O_4 nanocrystals. The variation of the polarity and size of the solvent molecules can also influence the spin-lattice relaxation dynamics. However, the effect is limited to the nanocrystals having sufficiently permeable surfactant layer, where the small solvent molecules (e.g. water) can access the surface and dynamically modify the ligand field on the surface.

The effect of surface-passivating surfactant and the surrounding medium on the relaxation rate of the excited state is an important topic in the research of various nanocrystalline materials and their applications.

---

* Reprinted in part with permission from Maiti, Sourav; Chen, Hsiang-Yun; Chen, Tai-Yen; Hsia, Chih-Hao; Son, Dong Hee. Effect of Surfactant and Solvent on Spin–Lattice Relaxation Dynamics of Magnetic Nanocrystals**.** *J. Phys. Chem. B* **2012,** *117* (16), 4399-4405. Copyright 2012 by the American Chemical Society

For instance, the relaxation of the photoexcited excitons or electrons in semiconducting or metallic nanocrystals, important in determining their photovoltaic and photocatalytic efficiency, is sensitive to the chemical environment at the nanocrystal surface.[96-98] For this reason, the effect of varying the surface-passivating molecules and the surrounding medium in the decay of the excited electronic states and phonons of the nanocrystals has been studied extensively.[35,99-102] In the case of semiconductor nanocrystals, significant effort was made in understanding the role of surfactant molecules in the charge transfer processes that affect the relaxation dynamics of the charge carriers.[6,34,36,103] The effect of the molecules in the solvent medium close to the nanocrystals that do not specifically bind to the nanocrystal surface on the dynamics of exciton relaxation through charge transfer or (and) energy transfer was also investigated.[60,104]

It was also recognized that the surfactant molecules can provide an extra vibrational bath for the nonradiative relaxation of the charge carriers in addition to the phonons of the nanocrystal lattice.[35] In metallic nanocrystals, the effect of varying the surrounding medium was mostly focused on phonon cooling that follows the rapid electron relaxation.[101] While the role of surface-passivating surfactant on the surface and surrounding medium in the electronic and phonon relaxation of the nanocrystals is relatively well studied, much less is known about their effect on the relaxation of the spin degrees of freedom. In magnetic nanocrystals of ferromagnetic metals and metal oxides, earlier studies investigated the effect of varying the surfactant molecules on the static magnetic properties. For instance, the role of surfactant molecules on restoring the

disordered surface spin and on the strength of surface spin-orbit coupling and surface anisotropy were investigated.[41,44,105] Recently, our group studied the dynamic magnetism of the optically excited $Fe_{3-x}Co_xO_4$ nanocrystals, where the rate of the recovery of magnetization following the optically induced demagnetization was measured as a function of particle size and chemical composition.[54] The rate of magnetization recovery occurring via spin-lattice relaxation became faster with decreasing particle size. This observation was explained by the average spin-orbit coupling having contribution from both the interior and the surface of the nanocrystals, where the surface experiences the stronger spin-orbit coupling than the interior part. Considering the surfactant's influence on the surface spin order and surface spin-orbit coupling, it is conceivable that varying the surfactant also influences the dynamics of spin-lattice relaxation in magnetic nanocrystals. Furthermore, if the solvent molecules can access the surface of the nanocrystals, they may also participate in the spin-lattice relaxation playing a similar role as the surface-bound surfactant molecules.

In this study, we examined whether varying the surfactant and solvent medium can influence the spin-lattice relaxation of the magnetic nanocrystals via time-resolved measurement of the magnetization in photoexcited Fe_3O_4 nanocrystals. Pump-probe Faraday rotation technique was used to measure the dynamics of the magnetization recovery following the pump-induced partial demagnetization. The results indicate that spin-lattice relaxation rate in Fe_3O_4 nanocrystals is affected by both the surface-binding functional groups of the surfactant molecules and surrounding solvent molecules. The influence of the solvent molecules on the spin-lattice relaxation is, however, more

apparent in the nanocrystals with thin surface passivation that allows the solvent molecules an easier access to the surface of the nanocrystals. The observation made in this study shows that the variation of the chemical environment on and near the surface of the magnetic nanocrystals can modify not only the static magnetic properties but also the dynamic magnetism.

5.2 Results and Discussion

5.2.1 Effect of Varying Surfactants on Spin-Lattice Relaxation

In order to examine whether varying the surface-binding functional group of the surfactant influences the dynamics of spin-lattice relaxation, we prepared Fe_3O_4 nanocrystals (5.3 nm in diameter) passivated with carboxylic acids and alcohols after phase transfer from the TMAH-passivated nanocrystals, as described in the experimental section. We chose these functional groups since the earlier study indicated that they exhibit different surface spin-orbit coupling resulting in the difference in the coercivity in $MnFe_2O_4$ nanocrystals.[44] For the surfactants with carboxyl group, oleic acid ($CH_3(CH_2)_7CH{=}CH(CH_2)_7CO_2H$) and 4-(octyloxy)benzoic acid ($CH_3(CH_2)_7OC_6H_4CO_2H$) were used. Octadecanol ($CH_3(CH_2)_{17}OH$) and 4-(n-octyloxy)phenol ($CH_3(CH_2)_7OC_6H_4OH$) were used as the surfactants having hydroxyl group. All of these surfactants produced highly dispersible nanocrystals in nonpolar solvents, which are consistent with relatively large free energy of adsorption ($-\Delta G$ = 14-18 kJ/mol,) of linear aliphatic acids and alcohols from n-heptane and n-decane to iron oxide surface.[106] This allowed us to examine the effect of varying the surfactant for the

sufficiently well isolated nanocrystals in dilute dispersion without the complication arising from the aggregates of the nanocrystals. The absence of aggregation was confirmed from the inspection of TEM images showing various different areas on the grid. Typical TEM images of the nanocrystals are shown in the figure 5.1.

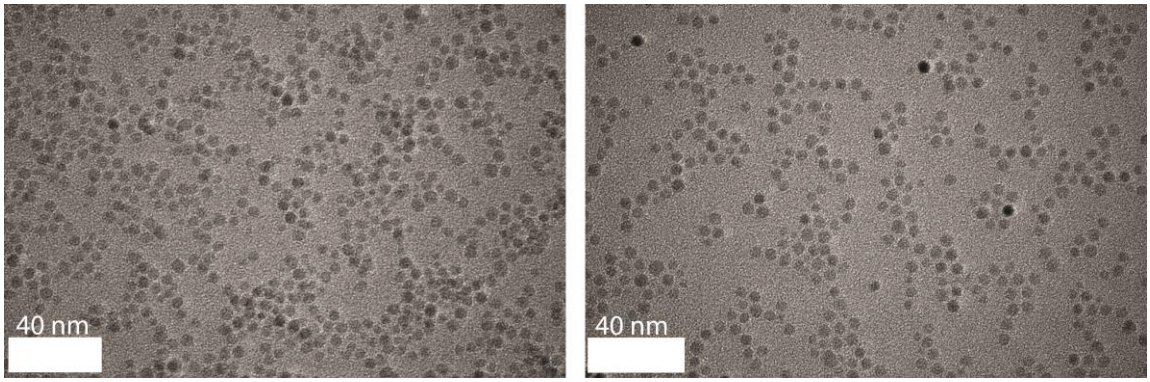

Figure 5.1 Typical TEM images of (a) octadecanol and (b) 4-(n-octyloxy)phenol-passivated Fe_3O_4 nanocrystals.

The interparticle magnetic dipolar interaction in the aggregate or assembly is known to change static magnetic properties.[71,107] Thiols, which are also known to passivate Fe_3O_4 surface, were not used in this study because of their higher tendency to form the aggregated nanocrystals. The optical absorption spectra of 1-octadecene solutions of Fe_3O_4 nanocrystals passivated with the four surfactants are almost identical throughout the visible and near infrared spectral region except in 4-(n-octyloxy)phenol-passivated nanocrystals (Fig 1(c)). The origin of a small additional absorption in visible region in 4-(n-octyloxy)phenol -passivated nanocrystals is not clear, while it may arise

from the charge transfer absorption between phenolic group and Fe^{3+} ion.[108] The absorption spectra of Fe_3O_4 nanocrystals are sensitive to the partial surface oxidation to Fe_2O_3 phase in >600 nm region, where the absorption from the intervalence charge transfer between Fe^{2+} and Fe^{3+} absorption becomes weaker with oxidation of Fe^{2+} to Fe^{3+}.[109] The similarity of the absorption spectra in this region in all the nanocrystal samples indicates that the degree of oxidation is maintained closely in all the samples during the surfactant exchange process.

Figure 5.2 (a) compares transient Faraday rotation data ($\Delta\theta/\theta_0$) of Fe_3O_4 nanocrystals passivated with four different surfactants and dispersed in 1-octadecene at the same concentration. We also compared the corresponding transient absorption data (ΔOD) to examine the effect of varying the surfactants on the electronic relaxation in Figure 5.2 (b). The recovery of $\Delta\theta/\theta_0$ represents the recovery of the magnetization following the photo-induced demagnetization by the pump pulse. The slower component of the recovery, occurring on hundreds of ps time scale, was assigned to the recovery of magnetization by spin-lattice relaxation in our earlier studies.[42,54] Therefore, we will compare the slower recovery component of $\Delta\theta/\theta_0$ to examine the effect of surface passivation on the dynamics of spin-lattice relaxation.

In Figure 5.2 (a), the nanocrystals passivated with alcohols exhibit the slower recovery of $\Delta\theta/\theta_0$ than those passivated with carboxylic acids. On the other hand, the difference in the tail group for a given surface-binding functional group has little influence on the dynamics. Variation of the surfactants also affects θ_0 that represents the relative static magnetization of the nanocrystals. Alcohol-passivated nanocrystals exhibit

~30 % smaller θ_0 than those passivated with carboxylic acids as shown in Table 1. Varying the tail group for a given surface-binding functional group does not affect θ_0. The surfactant molecule, although non-magnetic by itself, influences the total magnetization of the magnetic nanocrystals by partially reestablishing the order of the surface spins that would disorder in the absence of the surfactants.[41]

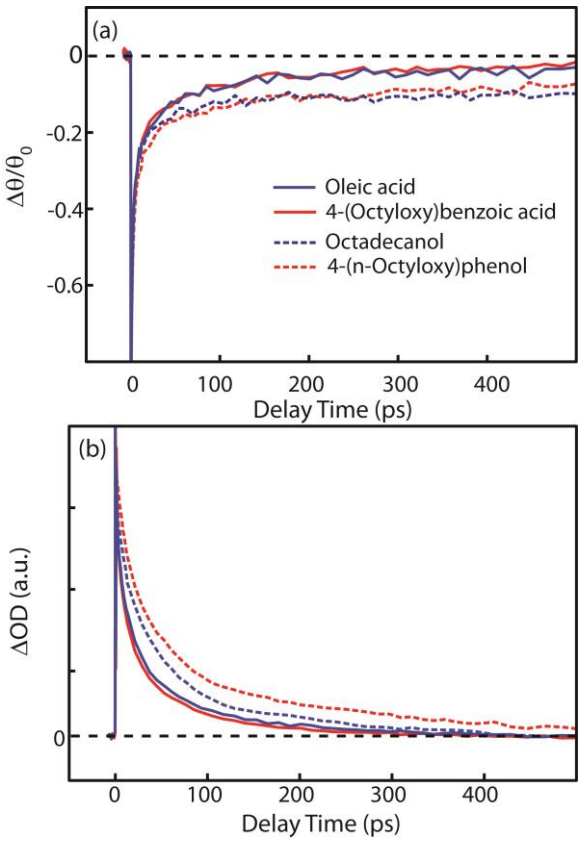

Figure 5.2 (a) Transient Faraday rotation and (b) transient absorption data of Fe_3O_4 nanocrystals passivated with four different surfactants and dispersed in 1-octadecene.

Solid and dashed lines are samples passivated with carboxylic acid and alcohols, respectively.

Therefore, the dependence of θ_0 on the surface-binding functional groups can be ascribed to the difference in the surfactant's capability to order the surface spins. The larger value of θ_0 for the carboxylic acid-passivated nanocrystals is also consistent with the carboxylic acid's particularly strong ability to restore the order in the surface spins due to its coordination character close to the lattice oxide.[41]

In principle, different surfactants can have different surface spin-orbit coupling or (and) vibronic coupling. Due to the relatively large surface to volume ratio of the nanocrystals of <10 nm, the differences in the surface can be seen in the experimentally measured overall spin-lattice relaxation rate.[42] Generally, as the strength of ligand field exerted on the magnetic ion becomes weaker, the effective spin-orbit coupling will become stronger and increase the spin-lattice relaxation rate.[110] Stronger vibronic coupling can increase spin-lattice relaxation rate as well. According to the study on the Langmuir adsorption isotherm of aliphatic alcohols and carboxylic acids to Fe_2O_3 surface from hydrocarbon solvent, carboxylic acids bind a bit more strongly than alcohols.[106] If one interprets the stronger binding as the stronger ligand field exerted to the metal ions on the surface, the slower recovery of $\Delta\theta/\theta_0$ in alcohol-passivated nanocrystals may seem in contradiction to the expectation based on the above argument. However, different surface coordination geometry (e.g., mixed bidentate[111,112] and monodentate binding of $-CO_2^-$ vs. monodentate binding of –OH) and possible differences in the surface grafting density and the vibronic coupling make the prediction

of the effect of surfactants on spin-lattice relaxation difficult. Furthermore, whether the difference in the surface spin disorder can influence the spin-lattice relaxation rate is another issue that adds the complexity to the problem. Nevertheless, the data shown in Figure 5.2 (a) clearly show that the surface-binding functional group can modify not only the static magnetization but also the rate of its relaxation in magnetic nanocrystals. Disentangling all the contributing factors determining the dynamics of spin-lattice relaxation in Fe_3O_4 nanocrystals passivated with different surfactants is beyond the scope of this study and will require further investigation.

The transient absorption (ΔOD) data shown in Figure 5.2 (b) indicate that varying the surfactants also influences the dynamics of electronic relaxation. The transitions excited by the pump pulse and monitored by the probe pulse correspond to the intervalence charge transfer between Fe^{2+} and Fe^{3+} ions.[113] In such case, the electronic relaxation occurring near the nanocrystal surface can be viewed as the photoinduced charge transfer process coupled to the nuclear motions of not only the lattice but also the surfactant molecules. Among the factors determining the rate of charge transfer, the vibrational organization energy associated with Fe-surfactant bonding is the most likely one that will vary with the nature of the surface-binding functional group. It is interesting to note that ΔOD data show a grouping based on the surface-binding functional group similarly to $\Delta\theta/\theta_0$ data. Oleic acid and 4-(octyloxy)benzoic acid-passivated nanocrystals exhibit very similar decay dynamics of $\Delta\theta/\theta_0$. In the two alcohol-passivated nanocrystals, while both exhibit the slower decay than the carboxylic acid-passivated nanocrystals, the difference in the dynamics is larger.

This is possibly due to the additional spectroscopic process probed in octyloxypheol-passivated nanocrystals as evidenced in the extra absorption in the visible region of the absorption spectrum shown in Figure 3.3 (c). Since both spin-lattice relaxation and electronic relaxation of Fe_3O_4 nanocrystals are affected by the nature of the bonding (e.g., strength and coordination geometry) between metal ions and the functional group, the similar grouping of the dynamics in both $\Delta\theta/\theta_0$ and ΔOD may not be surprising.

5.2.2 Effect of Varying Solvent on Spin-Lattice Relaxation

To investigate the effect of varying the surrounding solvent medium on the dynamics of spin-lattice relaxation, we prepared two groups of Fe_3O_4 nanocrystal samples (7.5 nm in diameter). One group of the samples (Group A) is the organic-soluble nanocrystals initially synthesized using oleic acid and oleylamine as the surfactants as described in the experimental section. Infrared spectroscopy confirmed the presence of carboxylate on the surface while the presence of oleylamine was unclear.[114] Group A represents the nanocrystals passivated with surfactants with long carbon-chain forming a relatively thick layer and soluble in organic solvents. Chloroform, iodopropane, cyclohexane and 1-octadecene were chosen as the solvents, since they encompass the varying degree of polarities and sizes with potentially different surface accessibility and surface-solvent interaction. For the second group (Group B), tetramethylammonium hydroxide (TMAH) was used as the surfactant to disperse the nanocrystals in the mixtures of water and propanol in varying proportions. Group B represents the nanocrystals passivated with a thin surfactant layer allowing the surface

more accessible to the solvent molecules. Short-chain carboxylic acids could not be used to prepare the nanocrystals with thin surfactant layer due to either nanocrystals chemical instability (e.g., dissolution by benzoic acid) or higher tendency to aggregate. The UV-Vis absorption spectra of the Group A and B samples are nearly identical as shown in Figure 3.3 (b) despite the large differences in the structure of the surfactant and solvent environment. The purpose of the comparison in these two groups of nanocrystals is to examine whether the solvent molecules can influence the spin-lattice relaxation, and how the structure of the surfactants affects the contribution of the solvent molecules to spin-lattice relaxation.

Figure 5.3 (a) and (b) show the transient Faraday rotation data ($\Delta\theta/\theta_0$) of Group A and B samples in various different solvents respectively. Figure 5.3 (c) and (d) are the corresponding transient absorption data. In Figure 5.3 (a), Group A samples having thick passivation exhibit essentially the same dynamics in $\Delta\theta/\theta_0$ data. The slow-recovery component has the time constant of ~250 ps for all three samples indicating that the solvent does not affect the spin-lattice relaxation rate in Group A samples. In a separate experiment, we made an additional comparison using iodopropane as the solvent. It has the highest dielectric constant (ε=7) among the solvents used for Group A samples and contains a heavier atom that can potentially have the stronger influence on the ligand field and spin-orbit coupling on the surface.

In this comparison, due to the relatively low solubility of the oleic acid-passivated nanocrystals in iodopropane, the comparison was made between octadecene and mixture of octadecene and iodopropane (15 and 26 volume % of iodopropane). The

recovery of $\Delta\theta/\theta_0$ signal in different solvent mixtures exhibited no noticeable difference (Figure 5.4), also indicating the absence of the influence from the solvent on the spin-lattice relaxation in Group A samples. ΔOD data shown in Figure 5.3 (c) are only weakly dependent on the solvent. The average decay time of the ΔOD signal varies slightly in the range of 61-53 ps. On the other hand, Group B samples passivated with TMAH exhibit quite different behavior from Group A samples in both $\Delta\theta/\theta_0$ and ΔOD data. In Figure 5.3 (b), the recovery of $\Delta\theta/\theta_0$ becomes significantly faster as the water content increases in the solvent. In 100% water, $\Delta\theta/\theta_0$ recovered nearly completely by 200 ps. The average decay time of ΔOD signal also became shorter by 40% (61 to 39ps) as the water content increased from 4 to 50%.

We ascribe the observed difference in the effect of the solvent on the spin-lattice relaxation in Group A and B samples mainly to the difference in the accessibility and affinity of the solvent molecules to the surface of the nanocrystals. In order for the solvent molecules to influence the spin-lattice relaxation, they should be sufficiently close to the magnetic ions on the surface to affect the surface spin-orbit coupling or (and) vibronic coupling. Since the oleyl group forms relatively well-passivating and thick surface layer, the penetration of the solvent molecules through the surfactant layer to the nanocrystal surface could be restricted for all the solvent molecules. In that case, varying the solvent in Group A samples will not change the surface coordination environment, therefore having little influence on the spin-lattice relaxation rate.

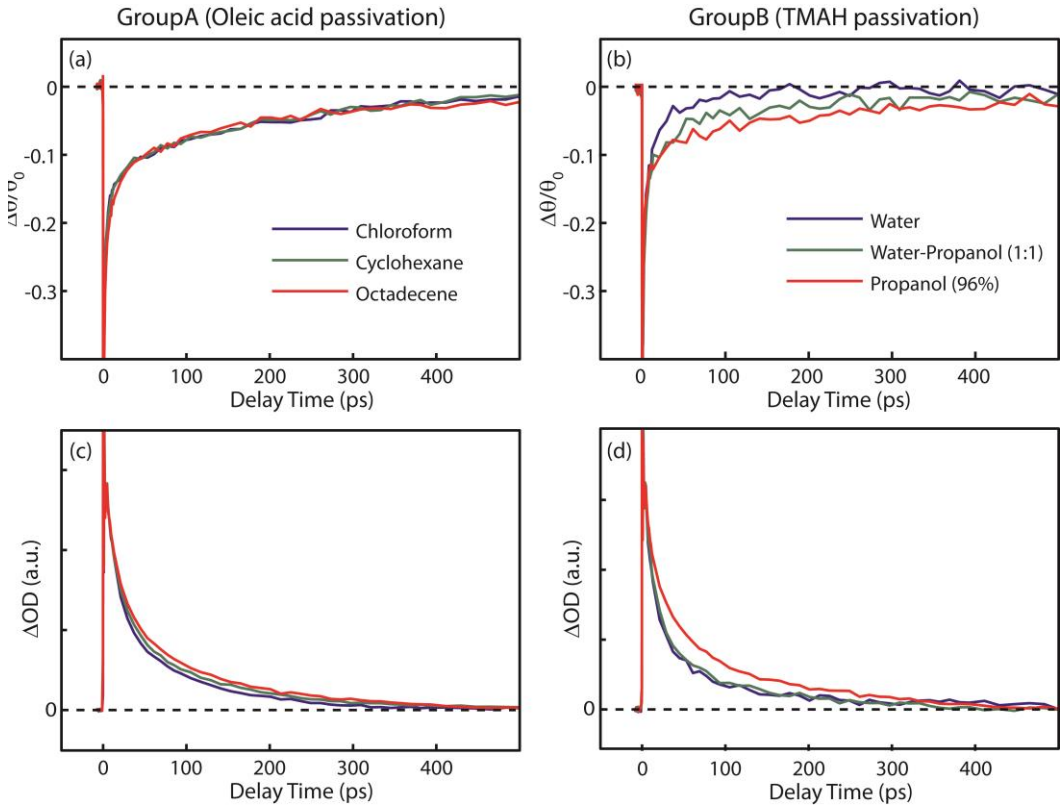

Figure 5.3 (a), (b) Transient Faraday rotation data of Group A and B nanocrystals, respectively. (c), (d) Transient absorption data of Group A and B nanocrystals, respectively.

In Group B samples, on the other hand, OH^- ions coordinate to the metal ions and tetramethylammonium cations form the outer layer.[115] Due to the relatively thin passivation layer formed by TMAH, solvent molecules may access the surface of the nanocrystals more readily in contrast to Group A samples. The stronger dependence of

the decay of ΔOD signal in Group B compared to Group A samples also corroborates the easier access of solvent molecules to TMAH –passivated surface. On the clean Fe_3O_4 surface exposed to the water vapor, dissociative chemisorption of water molecules into OH^- and H^+ occurs favorably during the initial phase of water adsorption followed by physisorption of water molecules at the higher coverage.[116] Since the surface of TMAH-passivated Fe_3O_4 nanocrystals is already sufficiently coordinated with OH^-, water molecules will likely physisorb on the surface. The enthalpy of desorption of physisorbed water molecules on the epitaxial Fe_3O_4 surface is ΔH_{des} = ~50 kJ/mol, which is larger than the enthalpy of vaporization of water (ΔH_{vap} = 44.0 kJ/mol).[117,118] Although ΔG of physisorption of a water molecule from the liquid water in the solvent to Fe_3O_4 surface is not available, the larger ΔH_{des} than ΔH_{vap} suggest that physisorption of water molecules can be favorable despite the strong hydrogen bonding present in bulk water. Since propanol and water have the same surface-binding functional group and similar ΔH_{vap} (ΔH_{vap} for propanol = 47.5 kJ/mol), it is reasonable to expect that propanol will adsorb similarly to water.[118] However, the overall capability to modify the surface coordination environment will vary depending on ΔG of adsorption and the accessibility of the solvent to the surface, which will be manifested as the difference in the solvent's effect on the spin-lattice relaxation rate. Therefore, one may view the solvent-dependent dynamics of spin-lattice relaxation observed in Group B samples from the perspective of the surface adsorption of different solvent molecules. As the water content in the solvent mixture increases in Group B samples, $\Delta\theta/\theta_0$ recovers more quickly as shown in Figure 5.3 (b), indicating enhanced spin-lattice relaxation with increasing water content.

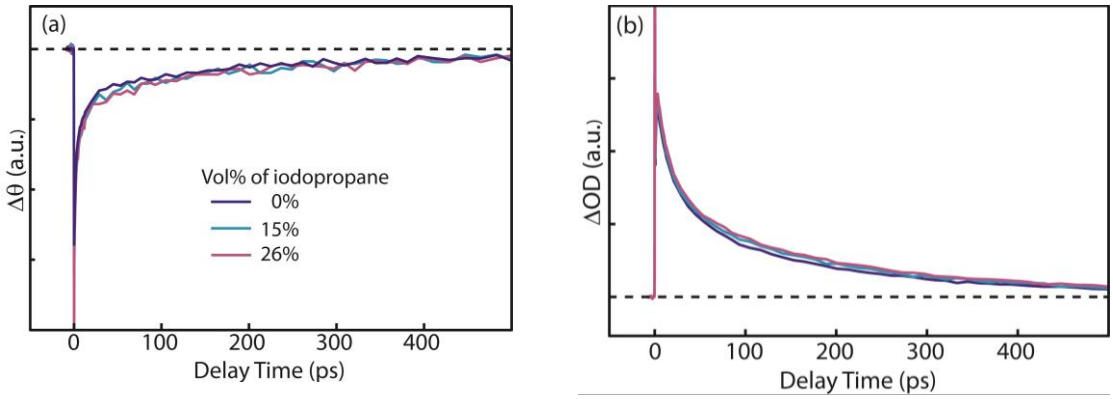

Figure 5.4 (a) Transient Faraday rotation and (b) transient absorption data of Fe_3O_4 nanocrystals (7 nm) with successive addition of iodopropane dispersed in 1-octadecene (pump fluence = 50 mJ/cm^2).

Potentially more active adsorption/desorption equilibrium of weakly-bound water molecules compared to OH^- may have contributed to the enhanced spin-lattice relaxation, since the fluctuation of the ligand field on the magnetic ion causes the spin-lattice relaxation.[119] Compared to water, propanol molecule is larger in size and its self-diffusion coefficient is ~4 times smaller.[120] This may impose a higher barrier for propanol molecule's access to the surface of the nanocrystals and lead to the slower fluctuation of the ligand field from the solvent molecules at the surface. In such case, the slower recovery of $\Delta\theta/\theta_0$ with the lower water content in the solvent may be ascribed to the propanol's poorer capability to access the surface and dynamically disturb the ligand field on the metal ions than water.

5.3 Conclusion

The effect of varying the surface-passivating surfactants and solvent environment on spin-lattice relaxation of the optically excited Fe_3O_4 nanocrystals has been investigated through the transient Faraday rotation measurement. The passivation of the nanocrystal surface with surfactants having different surface-binding functional groups (carboxylate vs. hydroxyl group) resulted in different spin-lattice relaxation rate, while the variation of tail group had no influence. The dependence of the spin-lattice relaxation on the surfactants is due to the differences in the metal-surfactant coordination strength and structure that affect the surface spin-orbit coupling or (and) vibronic coupling. The effect of varying the solvent environment for a given surface-passivating surfactant depends on the accessibility of the solvent molecules through the surfactant layer. The nanocrystals with thick and well-passivating layers experienced no effect of varying the solvent molecules of varying size and polarity. For the nanocrystals with thin and more permeable surfactant layer, such as TMAH, spin-lattice relaxation rate changed with the variation of the solvent composition.

CHAPTER VI

FUTURE ASPECTS: TEMPERATURE DEPENDENT Mn-LUMINESCENCE IN Mn-DOPED CdS/ZnS NANOCRYSTALS: ROLE OF TRAPPING ON Mn-LUMINESCENCE

We have investigated the temperature dependence of Mn-luminescence and lifetime in Mn-doped CdS/ZnS core/shell nanocrystals compared to the exciton emission in undoped nanocrystals elucidating the role of charge carrier trapping on dopant photoluminescence. Charge carrier trapping is the major process that hinders the photoluminescence of both undoped and doped nanocrystals, therefore, intensive research is going on to have better understanding of charge carrier trapping in nanocrystals.

Temperature dependent exciton luminescence intensity and lifetime have been studied on undoped nanocrystals in a wide temperature range starting from liquid He temperature to well above room temperature providing important information about major non-radiative processes within the nanocrystal. Four different temperature-dependent phenomena were observed in the case of CdSe nanocrystals. In very low temperature region (<50K) the exciton photoluminescence intensity remains constant with single exponential decay implying the radiative decay of exciton. In the region ~50-250K both the intensity and lifetime decreases with increasing temperature resulting dominated by thermally activated charge carrier trapping. In the region ~250 to 300K temperature induced anti-quenching is observed where the luminescence intensity and

lifetime increases with temperature due to reorganization on the nanocrystal surface induced by the surfactant phase transition. Above room temperature (>300), the luminescence intensity start to decrease due to thermal quenching that is explained by a trion formation mechanism. Here, electrons in the valence band are thermally promoted to surface states leaving hole in the valence band, thus photoexciton creates a trion and the nanocrystal undergoes non-radiative Auger relaxation. The exciton lifetime also start to decrease due more charge carrier trapping and creation of new trap states induced by enhanced temperature.To have more insight on charge carrier trapping Jones *et. al.* studied the temperature dependent exciton lifetime of CdSe/CdS/ZnS nanocrystals where they modeled the carrier trapping as an electron transfer process. They distinguished between surface traps and interfacial traps in a core/shell heterostructure. The exciton dynamics is mostly governed by the surface traps which have a broad energy distribution relative to the ground exciton energy and the charge carrier trapping-detrapping is the key contributing factor towards exciton lifetime.[121]

In the case of doped nanocrystals, exciton dynamics is greatly affected by the presence of dopant ions, for example in Mn-doped CdSe (diameter <~3.3 nm) the exciton emission is quenched due to exciton-Mn energy transfer which results in slowly decaying Mn-emission. Therefore, excitonic lifetime becomes faster (from ns to ps) and exciton-intensity is quenched accompanied by a low energy Mn-emission. Temperature dependence of Mn-doped CdSe (diameter ~2.2 nm) has revealed that the slowly decaying Mn can act as energy storage and transfer the population back to exciton with increasing temperature. Therefore, in the 5-185K range, both exciton emission intensity

and lifetime increases with temperature. The Mn-emission intensity and lifetime decreases with temperature presumably due to increase in non-radiative rates for Mn-decay. This back energy transfer from excited Mn to repopulate excitonic states has been used to make dual emitting ZnMnSe/ZnCdSe core/shell nanocrystals where the ratio between exciton emission and Mn-emission can be tuned by temperature.[122] Due to back energy transfer, increasing temperature leads to increase in exciton-photoluminescence with simultaneous decrease in Mn-luminescence. Therefore, temperature dependent luminescence studies can provide insight about energy transfer dynamics in doped nanocrystals.

Recently, we have explored the dynamics of exciton-Mn energy transfer in CdS/ZnS core/shell nanocrystals by varying the Mn-concentration and doping location. It was found that energy transfer dynamics strongly depends on hole trapping, where hole trapping competes with the exciton-Mn energy transfer. Hole trapping blocks the exciton-Mn energy transfer and subsequently decreases the Mn-luminescence quantum yield as Mn-quantum yield depends on the extent of energy transfer from exciton to Mn. As discussed earlier, temperature dependent luminescence studies provide important information about charge carrier trapping, we intend to investigate the temperature dependence of Mn-luminescence compared to the undoped counterpart to shed more light on the effect of hole trapping on Mn-luminescence. Also, it will be important to study the role of surfactant here. After adding hole trapping octanethiol in Mn-doped nanocrystals, increase in Mn-emission was observed due to back energy transfer from

thiol traps. Temperature dependent studies after thiol exchange will be helpful to provide more insight about hole trapping dynamics.

REFERENCES

(1) Brus, L. E. *J. Chem. Phys.* **1983**, *79*, 5566.

(2) Alivisatos, A. P. *Science* **1996**, *271*, 933.

(3) Nozik, A. *Annu. Rev. Phys. Chem.* **2001**, *52*, 193.

(4) Murray, C. B.; Norris, D. J.; Bawendi, M. G. *J. Am. Chem. Soc.* **1993**, *115*, 8706.

(5) Klimov, V. I.; McBranch, D. W.; Leatherdale, C. A.; Bawendi, M. G. *Phys. Rev. B* **1999**, *60*, 13740.

(6) Klimov, V. I.; Mikhailovsky, A. A.; McBranch, D. W.; Leatherdale, C. A.; Bawendi, M. G. *Phys. Rev. B* **2000**, *61*, R13349.

(7) Klimov, V. I.; Schwarz, C. J.; McBranch, D. W.; Leatherdale, C. A.; Bawendi, M. G. *Phys. Rev. B* **1999**, *60*, R2177.

(8) Kambhampati, P. *Acc. Chem. Res.* **2010**, *44*, 1.

(9) Talapin, D. V.; Lee, J.-S.; Kovalenko, M. V.; Shevchenko, E. V. *Chem. Rev.* **2009**, *110*, 389.

(10) Kamat, P. V. *J. Phys. Chem. C* **2008**, *112*, 18737.

(11) Robel, I.; Subramanian, V.; Kuno, M.; Kamat, P. V. *J. Am. Chem. Soc.* **2006**, *128*, 2385.

(12) Colvin, V. L.; Schlamp, M. C.; Alivisatos, A. P. *Nature* **1994**, *370*, 354.

(13) Bruchez, M.; Moronne, M.; Gin, P.; Weiss, S.; Alivisatos, A. P. *Science* **1998**, *281*, 2013.

(14) Smith, A. M.; Duan, H.; Mohs, A. M.; Nie, S. *Adv. Drug Delivery Rev.* **2008**, *60*, 1226.

(15) El-Sayed, M. A. *Acc. Chem. Res.* **2004**, *37*, 326.

(16) Peng, Z. A.; Peng, X. *J. Am. Chem. Soc.* **2000**, *123*, 183.

(17) Yu, W. W.; Peng, X. *Angew. Chem. Int. Ed.* **2002**, *41*, 2368.

(18) Jun, S.; Jang, E. *Angew. Chem. Int. Ed.* **2013**, *52*, 679.

(19) Park, J.; Joo, J.; Kwon, S. G.; Jang, Y.; Hyeon, T. *Angew. Chem. Int. Ed.* **2007**, *46*, 4630.

(20) Beaulac, R.; Ochsenbein, S. T.; Gamelin, D. R. In *Nanocrystal Quantum Dots*; Klimov, V. I., Ed.; CRC Press: Boca Raton, FL, 2010; Vol. 2nd p397.

(21) Pradhan, N.; Sarma, D. D. *J. Phys. Chem. Lett.* **2011**, *2*, 2818.

(22) Manna, G.; Jana, S.; Bose, R.; Pradhan, N. *J. Phys. Chem. Lett.* **2012**, *3*, 2528.

(23) Beaulac, R.; Archer, P. I.; Ochsenbein, S. T.; Gamelin, D. R. *Adv. Funct. Mater.* **2008**, *18*, 3873.

(24) Sarkar, S.; Karan, N. S.; Pradhan, N. *Angew. Chem. Int. Ed.* **2011**, *50*, 6065.

(25) Norris, D. J.; Efros, A. L.; Erwin, S. C. *Science* **2008**, *319*, 1776.

(26) Erwin, S. C.; Zu, L.; Haftel, M. I.; Efros, A. L.; Kennedy, T. A.; Norris, D. J. *Nature* **2005**, *736*, 91.

(27) Beaulac, R.; Archer, P. I.; Gamelin, D. R. *J. Solid State Chem.* **2008**, *181*, 1582.

(28) Beaulac, R.; Archer, P. I.; van Rijssel, J.; Meijerink, A.; Gamelin, D. R. *Nano Lett.* **2008**, *8*, 2949.

(29) Archer, P. I.; Santangelo, S. A.; Gamelin, D. R. *Nano Lett.* **2007**, *7*, 1037.

(30) Bussian, D. A.; Crooker, S. A.; Yin, M.; Brynda, M.; Efros, A. L.; Klimov, V. I. *Nat. Mater.* **2009**, *8*, 35.

(31) Bryan, J. D.; Heald, S. M.; Chambers, S. A.; Gamelin, D. R. *J. Am. Chem. Soc.* **2004**, *126*, 11640.

(32) Chen, H.-Y.; Maiti, S.; Son, D. H. *ACS Nano* **2012**, *6*, 583.

(33) Beaulac, R.; Archer, P. I.; Liu, X.; Lee, S.; Salley, G. M.; Dobrowolska, M.; Furdyna, J. K.; Gamelin, D. R. *Nano Lett.* **2008**, *8*, 1197.

(34) Knowles, K. E.; Frederick, M. T.; Tice, D. B.; Morris-Cohen, A. J.; Weiss, E. A. *J. Phys. Chem. Lett.* **2012**, *3*, 18.

(35) Guyot-Sionnest, P.; Wehrenberg, B.; Yu, D. *J. Chem. Phys.* **2005**, *123*, 074709.

(36) Pandey, A.; Guyot-Sionnest, P. *Science* **2008**, *322*, 929.

(37) Burda, C.; Link, S.; Mohamed, M.; El-Sayed, M. *J. Phys. Chem. B* **2001**, *105*, 12286.

(38) Gradmann, U. *J. Magn. Magn. Mater.* **1991**, *100*, 481.

(39) Tronc, E.; Ezzir, A.; Cherkaoui, R.; Chanéac, C.; Noguès, M.; Kachkachi, H.; Fiorani, D.; Testa, A. M.; Grenèche, J. M.; Jolivet, J. P. *J. Magn. Magn. Mater.* **2000**, *221*, 63.

(40) Respaud, M.; Broto, J. M.; Rakoto, H.; Fert, A. R.; Thomas, L.; Barbara, B.; Verelst, M.; Snoeck, E.; Lecante, P.; Mosset, A.; Osuna, J.; Ely, T. O.; Amiens, C.; Chaudret, B. *Phys. Rev. B* **1998**, *57*, 2925.

(41) Salafranca, J.; Gazquez, J.; Pérez, N.; Labarta, A.; Pantelides, S. T.; Pennycook, S. J.; Batlle, X.; Varela, M. *Nano Lett.* **2012**, *12*, 2499.

(42) Hsia, C.-H.; Chen, T.-Y.; Son, D. H. *J. Am. Chem. Soc.* **2009**, *131*, 9146.

(43) Gazeau, F.; Bacri, J. C.; Gendron, F.; Perzynski, R.; Raikher, Y. L.; Stepanov, V. I.; Dubois, E. *J. Magn. Magn. Mater.* **1998**, *186*, 175.

(44) Vestal, C. R.; Zhang, Z. J. *J. Am. Chem. Soc.* **2003**, *125*, 9828.

(45) Guyot-Sionnest, P.; Hines, M. A. *Appl. Phys. Lett.* **1998**, *72*, 686.

(46) Guyot-Sionnest, P.; Shim, M.; Matranga, C.; Hines, M. *Phys. Rev. B* **1999**, *60*, R2181.

(47) Burda, C.; Green, T. C.; Link, S.; El-Sayed, M. A. *J. Phys. Chem. B* **1999**, *103*, 1783.

(48) Sewall, S. L.; Cooney, R. R.; Anderson, K. E. H.; Dias, E. A.; Kambhampati, P. *Phys. Rev. B* **2006**, *74*, 235328.

(49) Cooney, R. R.; Sewall, S. L.; Dias, E. A.; Sagar, D. M.; Anderson, K. E. H.; Kambhampati, P. *Phys. Rev. B* **2007**, *75*, 245311.

(50) Kaniyankandy, S.; Rawalekar, S.; Verma, S.; Palit, D. K.; Ghosh, H. N. *Phys. Chem. Chem. Phys.* **2010**, *12*, 4210.

(51) Rawalekar, S.; Kaniyankandy, S.; Verma, S.; Ghosh, H. N. *J. Phys. Chem. C* **2009**, *114*, 1460.

(52) Chen, H.-Y.; Chen, T.-Y.; Son, D. H. *J. Phys. Chem. C* **2010**, *114*, 4418.

(53) Hsia, C.-H.; Chen, T.-Y.; Son, D. H. *Nano Lett.* **2008**, *8*, 571.

(54) Chen, T.-Y.; Hsia, C.-H.; Chen, H.-Y.; Son, D. H. *J. Phys. Chem. C* **2010**, *114*, 9713.

(55) Norris, D. J. In *Nanocrystal Quantum Dots*; Klimov, V. I., Ed.; CRC Press: Boca Raton,FL, 2010; Vol. 2nd, p 63.

(56) Heim, U.; Wiesner, P. *Phys. Rev. Lett.* **1973**, *30*, 1205.

(57) Sewall, S. L.; Cooney, R. R.; Anderson, K. E. H.; Dias, E. A.; Sagar, D. M.; Kambhampati, P. *J. Chem. Phys.* **2008**, *129*, 084701.

(58) Klimov, V. I. *J. Phys. Chem. B* **2000**, *104*, 6112.

(59) Knowles, K. E.; McArthur, E. A.; Weiss, E. A. *ACS Nano* **2011**, *5*, 2026.

(60) Boulesbaa, A.; Huang, Z.; Wu, D.; Lian, T. *J. Phys. Chem. C* **2009**, *114*, 962.

(61) McArthur, E. A.; Morris-Cohen, A. J.; Knowles, K. E.; Weiss, E. A. *J. Phys. Chem. B* **2010**, *114*, 14514.

(62) Green, M. *J. Mater. Chem.* **2010**, *20*, 5797.

(63) Pradhan, N.; Peng, X. *J. Am. Chem. Soc.* **2007**, *129*, 3339.

(64) Yang, Y.; Chen, O.; Angerhofer, A.; Cao, Y. C. *Chem. Eur. J.* **2009**, *15*, 3186.

(65) Chen, T.-Y. In *Electronic and Magnetization Dynamics of Cobalt Substituted Iron Oxide Nanocrystals (Doctoral dissertation)*; Texas A&M University: Texas, 2010.

(66) Hsia, C.-H. In *Studies of Optically Induced Magnetization Dynamics in Colloidal Iron Oxide Nanocrystals (Doctoral dissertation)*; Texas A&M University: 2010.

(67) Yang, Y.; Chen, O.; Angerhofer, A.; Cao, Y. C. *J. Am. Chem. Soc.* **2006**, *128*, 12428.

(68) Sun, S.; Zeng, H. *J. Am. Chem. Soc.* **2002**, *124*, 8204.

(69) Jia, S.; Hsia, C.-H.; Son, D. H. *J. Phys. Chem. C* **2011**, *115*, 92.

(70) Chen, T.-Y.; Hsia, C.-H.; Son, D. H. *J. Phys. Chem. C* **2008**, *112*, 10125.

(71) Vestal, C. R.; Song, Q.; Zhang, Z. J. *J. Phys. Chem. B* **2004**, *108*, 18222.

(72) Vlaskin, V. A.; Janssen, N.; van Rijssel, J.; Beaulac, R.; Gamelin, D. R. *Nano Lett.* **2010**, *10*, 3670.

(73) Beaulac, R.; Schneider, L.; Archer, P. I.; Bacher, G.; Gamelin, D. R. *Science* **2009**, *325*, 973.

(74) Wood, V.; Halpert, J. E.; Panzer, M. J.; Bawendi, M. . ulovi , . *Nano Lett.* **2009**, *9*, 2367.

(75) Wuister, S. F.; de Mello Donegá, C.; Meijerink, A. *J. Phys. Chem. B* **2004**, *108*, 17393.

(76) Suyver, J. F.; Wuister, S. F.; Kelly, J. J.; Meijerink, A. *Phys. Chem. Chem. Phys.* **2000**, *2*, 5445.

(77) Chen, O.; Yang, Y.; Wang, T.; Wu, H.; Niu, C.; Yang, J.; Cao, Y. C. *J. Am. Chem. Soc.* **2011**, *133*, 17504.

(78) Frederick, M. T.; Amin, V. A.; Cass, L. C.; Weiss, E. A. *Nano Lett.* **2011**, *11*, 5455.

(79) Frederick, M. T.; Amin, V. A.; Weiss, E. A. *J. Phys. Chem. Lett.*, 634.

(80) Pradhan, N.; Battaglia, D. M.; Liu, Y.; Peng, X. *Nano Lett.* **2006**, *7*, 312.

(81) Rogach, A. L.; Kornowski, A.; Gao, M.; Eychmüller, A.; Weller, H. *J. Phys. Chem. B* **1999**, *103*, 3065.

(82) Gill, R.; Willner, I.; Shweky, I.; Banin, U. *J. Phys. Chem. B* **2005**, *109*, 23715.

(83) Bullen, C.; Mulvaney, P. *Langmuir* **2006**, *22*, 3007.

(84) Munro, A. M.; Jen-La Plante, I.; Ng, M. S.; Ginger, D. S. *J. Phys. Chem. C* **2007**, *111*, 6220.

(85) Liu, I. S.; Lo, H.-H.; Chien, C.-T.; Lin, Y.-Y.; Chen, C.-W.; Chen, Y.-F.; Su, W.-F.; Liou, S.-C. *J. Mater. Chem.* **2008**, *18*, 675.

(86) Munro, A. M.; Ginger, D. S. *Nano Lett.* **2008**, *8*, 2585.

(87) Pong, B.-K.; Trout, B. L.; Lee, J.-Y. *Langmuir* **2008**, *24*, 5270.

(88) Wang, Q.; Xu, Y.; Zhao, X.; Chang, Y.; Liu, Y.; Jiang, L.; Sharma, J.; Seo, D.-K.; Yan, H. *J. Am. Chem. Soc.* **2007**, *129*, 6380.

(89) Barkhouse, D. A. R.; Pattantyus-Abraham, A. G.; Levina, L.; Sargent, E. H. *ACS Nano* **2008**, *2*, 2356.

(90) Rogach, A. L.; Franzl, T.; Klar, T. A.; Feldmann, J.; Gaponik, N.; Lesnyak, V.; Shavel, A.; Eychmüller, A.; Rakovich, Y. P.; Donegan, J. F. *J. Phys. Chem. C* **2007**, *111*, 14628.

(91) Jeong, S.; Achermann, M.; Nanda, J.; Ivanov, S.; Klimov, V. I.; Hollingsworth, J. A. *J. Am. Chem. Soc.* **2005**, *127*, 10126.

(92) Zheng, J.; Gao, F.; Wei, G.; Yang, W. *Chem. Phys. Lett.* **2012**, *519–520*, 73.

(93) Sarkar, S.; Patra, B. K.; Guria, A. K.; Pradhan, N. *J. Phys. Chem. Lett.* **2013**, *4*, 2084.

(94) Ithurria, S.; Guyot-Sionnest, P.; Mahler, B.; Dubertret, B. *Phys. Rev. Lett.* **2007**, *99*, 265501.

(95) Chen, H.-Y.; Maiti, S.; Nelson, C. A.; Zhu, X.; Son, D. H. *J. Phys. Chem. C* **2012**, *116*, 23838.

(96) Kamat, P. V. *Acc. Chem. Res.* **2012**, *45*, 1906.

(97) Nozik, A. J.; Beard, M. C.; Luther, J. M.; Law, M.; Ellingson, R. J.; Johnson, J. C. *Chem. Rev.* **2010**, *110*, 6873.

(98) Wu, K.; Zhu, H.; Liu, Z.; Rodríguez-Córdoba, W.; Lian, T. *J. Am. Chem. Soc.* **2012**, *134*, 10337.

(99) Hyun, B.-R.; Bartnik, A. C.; Lee, J.-K.; Imoto, H.; Sun, L.; Choi, J. J.; Chujo, Y.; Hanrath, T.; Ober, C. K.; Wise, F. W. *Nano Lett.* **2009**, *10*, 318.

(100) Losego, M. D.; Grady, M. E.; Sottos, N. R.; Cahill, D. G.; Braun, P. V. *Nat. Mater.* **2012**, *11*, 502.

(101) Link, S.; Furube, A.; Mohamed, M. B.; Asahi, T.; Masuhara, H.; El-Sayed, M. A. *J. Phys. Chem. B* **2002**, *106*, 945.

(102) Hartland, G. V. *Chem. Rev.* **2011**, *111*, 3858.

(103) Kambhampati, P. *J. Phys. Chem. C* **2011**, *115*, 22089.

(04) a ng, . odr guez-C r doba, . ian, T. *J. Am. Chem. Soc.* **2011**, *133*, 9246.

(105) Guardia, P.; Batlle-Brugal, B.; Roca, A. G.; Iglesias, O.; Morales, M. P.; Serna, C. J.; Labarta, A.; Batlle, X. *J. Magn. Magn. Mater.* **2007**, *316*, e756.

(106) Bellobono, I. R.; Selli, E.; Righetto, L.; Muffato, F.; Ermondi, C. *Mater. Chem. Phys.* **1989**, *21*, 155.

(107) Chen, J.; Dong, A.; Cai, J.; Ye, X.; Kang, Y.; Kikkawa, J. M.; Murray, C. B. *Nano Lett.* **2010**, *10*, 5103.

(108) Mayilmurugan, R.; Visvaganesan, K.; Suresh, E.; Palaniandavar, M. *Inorg. Chem.* **2009**, *48*, 8771.

(109) Tang, J.; Myers, M.; Bosnick, K. A.; Brus, L. E. *J. Phys. Chem. B* **2003**, *107*, 7501.

(110) Stöhr, J.; Siegmann, H. C. In *Magnetism: From Fundamentals to Nanoscale Dynamics*; Springer: Berlin, Germany, 2006.

(111) Polito, L.; Colombo, M.; Monti, D.; Melato, S.; Caneva, E.; Prosperi, D. *J. Am. Chem. Soc.* **2008**, *130*, 12712.

(112) Zhang, L.; He, R.; Gu, H.-C. *Appl. Surf. Sci.* **2006**, *253*, 2611.

(113) He, Y. P.; Miao, Y. M.; Li, C. R.; Wang, S. Q.; Cao, L.; Xie, S. S.; Yang, G. Z.; Zou, B. S.; Burda, C. *Phys. Rev. B* **2005**, *71*, 125411.

(114) Klokkenburg, M.; Hilhorst, J.; Erné, B. H. *Vib. Spectrosc* **2007**, *43*, 243.

(115) Cheng, F.-Y.; Su, C.-H.; Yang, Y.-S.; Yeh, C.-S.; Tsai, C.-Y.; Wu, C.-L.; Wu, M.-T.; Shieh, D.-B. *Biomaterials* **2005**, *26*, 729.

( ) Tomb c z, . a d , A. Ill s, . szl , . a rberoglio, . J edlovszky, . *Langmuir* **2009**, *25*, 13007.

(117) Joseph, Y.; Kuhrs, C.; Ranke, W.; Weiss, W. *Surf. Sci.* **1999**, *433–435*, 114.

(118) In *CRC Handbook of Chemistry and Physics. Section 6. Enthalpy of Vaporization*; 92nd ed.; Taylor & Francis Group: Boca Raton, FL, 2012.

(119) Shrivastava, K. N. *Physica Status Solidi B* **1983**, *117*, 437.

(120) Pratt, K. C.; Wakeham, W. A. *J. Chem. Soc., Faraday Trans. 2* **1977**, *73*, 997.

(121) Jones, M.; Lo, S. S.; Scholes, G. D. *Proc. Natl. Acad. Sci.* **2009**, *106*, 3011.

(122) Vlaskin, V. A.; Beaulac, R.; Gamelin, D. R. *Nano Lett.* **2009**, *9*, 4376.

APPENDIX

Fitting equation for transient absorption data:

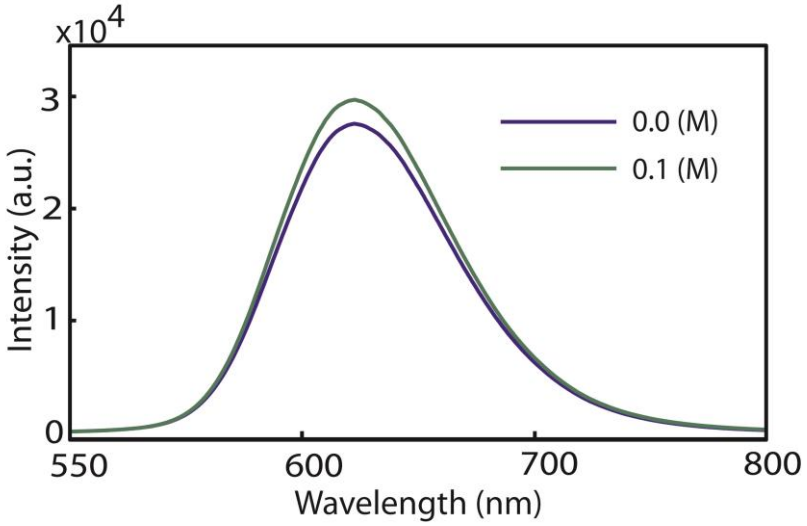

Figure A1. Mn-PL spectra for interfacial doped nanocrystal in presence of octanethiol which does not show any wavelength dependence of Mn-PL in presence of octanethiol.

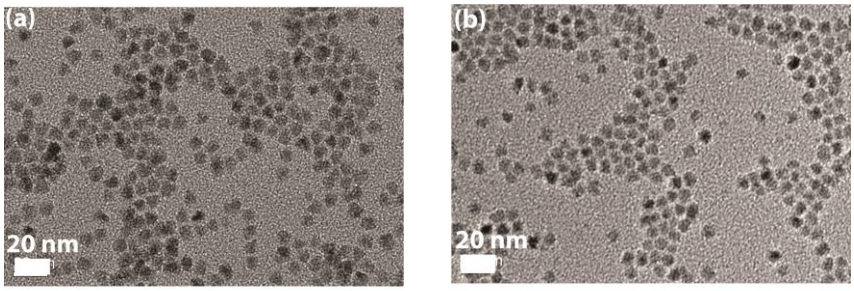

Figure A2. TEM image of (a) interfacial and (b) 2nd layer Mn-doped CdS/ZnS.

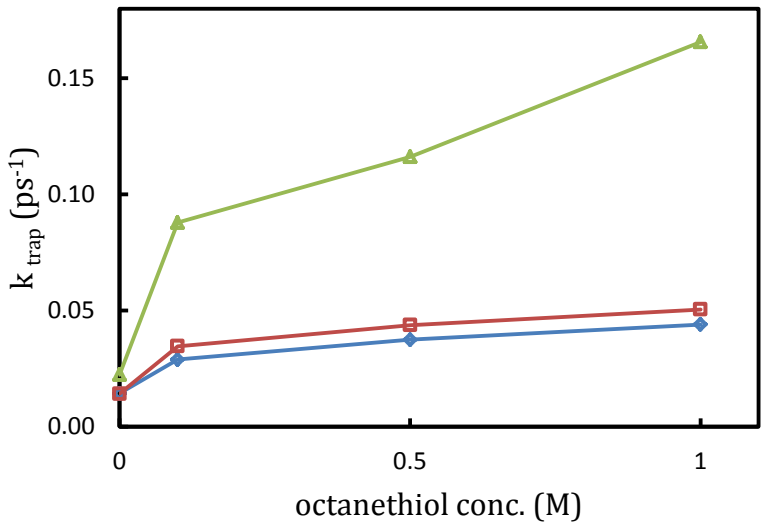

Figure A3. Hole trapping rate (k_{trap}) for interfacial doped (□), 2nd layer doped (◇) and thin shell (△) nanocrystal from bleach recovery measurements.

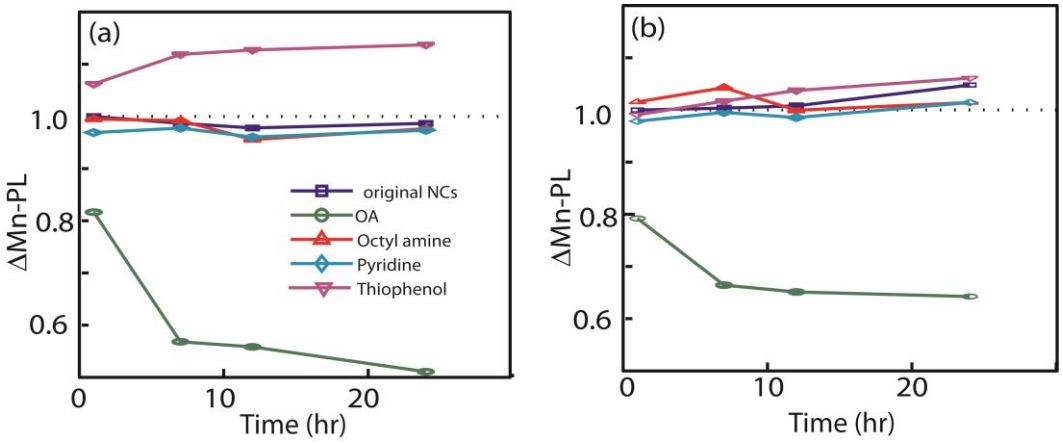

Figure A4. Effect of Different Surfactants on Mn-PL in (a) interfacial (19Mn) and (b) 2nd layer (15Mn) doped nanocrystals.

Sample	a_1	a_2	a_3	τ_1 (ps)	τ_2 (ps)	$\tau_{avg} = \tau_{ET}$ (ps)	τ_{trap} (ps)	τ_{OT} (ps)
Interfacial Mn-doed CdS/ZnS	0. 0	0.3	0.089	0.73	9.0	.99	70.	-
0. (M) thiol	0.58	0.25	0.	0. 7	7.3	5.75	28.9	48.9
0.5(M) thiol	0.5	0.25	0. 89	0. 8	5.57	5.33	22.9	33.8
(M) thiol	0.55	0.24	0.207	0.72	5.52	5. 7	9.8	27.5

Table A1. Fitting parameters for interfacial Mn-doped CdS/ZnS.